Coverage Analysis of Multiuser Visible Light Communication Networks

Coverage Analysis of Multiuser Visible Light Communication Networks

Liang Yin and Harald Haas, *Senior Member, IEEE*

***Abstract*— In this paper, a new mathematical framework for the coverage probability analysis of multiuser visible light communication (VLC) networks is presented. It takes into account the idle probability of access points (APs) that are not associated with any users and hence do not function as the source of interference. The idle probability of APs is evident especially in underloaded networks as well as general networks that operate with an AP sleep strategy to save energy and/or minimize the co-channel interference. Due to the absence of the "multipath fading" effect, the evaluation of the distribution function of the signal-to-interference-plus-noise ratio (SINR) is more challenging in VLC networks than in radio frequency-based cellular networks. By using the statistical-equivalent transformation of the SINR, analytical expressions for the coverage probability are derived and given in tractable forms. Comparing the derived results with extensive Monte Carlo simulations, we show that assuming a thinned homogeneous Poisson point process for modeling active APs is valid in general, and it gives close results to the exact ones when the density of users is no less than the density of APs in the network. Both analytical and simulation results show that, for typical receiver noise levels (~ -117 dBm), approximating the SINR by the signal-to-interference ratio is sufficiently accurate for the coverage analysis in VLC networks.**

***Index Terms*— Visible light communication, light-emitting diode, coverage probability, Poisson point process, stochastic geometry.**

I. Introduction

CURRENT wireless networks are experiencing difficulties in keeping pace with the exponential growth of wireless devices that require higher data rate and seamless service coverage. Such imminent problems have motivated many industry partners and research communities to seek new technologies for wireless communication. Among many candidate solutions, visible light communication (VLC) [1]–[3] has been acknowledged as a promising technology to address the scarcity of radio frequency (RF) spectra, due to its advantages in modulation bandwidth, data rate, frequency reuse factor and link security. Extensive studies on point-to-point VLC transmission and reception techniques during the past decade have also led to the recent standardization of VLC for short-range applications: IEEE 802.15.7 [4]. A revision to the current standard is also in progress.

Small-cell deployment for heterogeneous cellular networks has proven to be effective in improving the network throughput and spectral efficiency. The femtocell-like deployment of VLC in indoor environments leads to the concept of optical attocells [5], where each light-emitting diode (LED) acts as an optical access point (AP) to serve multiple users within its coverage. Since then, many research efforts have been given to the design and analysis of multiuser VLC networks. Topics include multiple-input multiple-output (MIMO) transmission [6], transceiver design [7], precoder and equalizer design [8], AP coordination [9], interference mitigation [10], user scheduling [11] and resource allocation and optimization [12], [13], to name just a few.

A. Related Work and Motivation

System-level performance of multiuser VLC networks is typically evaluated with the aid of computer simulations. They are often complicated, time-consuming and unable to provide many insights into how the performance is affected by various parameters in the network. The analytical evaluation, on the other hand, is generally not straightforward due to the lack of accurate and at the same time analytically tractable models. The most common approach for modeling the location of optical APs is based on the grid model, where LED lights are installed in the ceiling with a regular pattern [1], [2], [6], [9], [13], [14]. The evaluation of the grid based network is recognized to be analytically difficult and hence is normally done with computer simulation, which has also motivated the authors in [14] to use stochastic models [15]–[18] for the performance evaluation. Compared to the grid model, stochastic models are more mathematically tractable. More importantly, the following observations indicate that in some scenarios a stochastic model is required in order to accurately characterize the performance of VLC networks. Firstly, modern LED lights with built-in motion detection sensors are widely deployed in public spaces to reduce energy consumption. In this scenario, some of the LED lights are temporarily switched off when they are not required to provide illumination. Also, even when switched on, some of the LEDs can turn off their wireless communication functionality when no data traffic is demanded from them, for

Manuscript received May 3, 2017; revised September 27, 2017; accepted December 8, 2017. The work of H. Haas was supported by the U.K. Engineering and Physical Sciences Research Council under Grant EP/K008757/1. The associate editor coordinating the review of this paper and approving it for publication was M. Uysal. *(Corresponding author: Liang Yin.)*

The authors are with the Li-Fi Research and Development Centre, School of Engineering, Institute for Digital Communications, The University of Edinburgh, Edinburgh EH9 3JL, U.K. (e-mail: l.yin@ed.ac.uk; h.haas@ed.ac.uk).

Color versions of one or more of the figures in this paper are available online at http://ieeexplore.ieee.org.

Digital Object Identifier 10.1109/TWC.2017.2782694

example, relying on an AP sleep strategy. In these scenarios, the distribution of APs cannot be accurately modeled by the grid model. Instead, a stochastic thinning process built upon the grid-like deployment of LEDs is more accurate. However, modeling this stochastic thinning process requires full knowledge of the users' movement and handover characteristics, which is not analytically tractable. Secondly, the distribution of active APs in a VLC network is generally variable, and it changes dynamically due to the random movement of users. Thirdly, the grid model is not applicable in scenarios where not only ceiling lights but also LED screens, reading lamps, and other "smart" lights are an integral part of the network architecture, in which the deployment of VLC APs appears to be more stochastic. For these reasons and in order to obtain analytically tractable results, the PPP model is of our focus in this work.

To the best of authors' knowledge, [14] is the only published work that reports on the performance of multiuser VLC networks using the stochastic model. The distribution function of the signal-to-interference-plus-noise ratio (SINR) of a typical user in the network reported in [14] was given as a sum of Gamma densities, whose calculation requires Gram-Charlier series expansion with infinite terms and Laguerre polynomials. As a result, computing the distribution function of the SINR would involve complicated integrals and infinite sums. Motivated by this, we report in this paper a new and simpler method for the characterization of the density function of the SINR by exploring powerful mathematical tools from stochastic geometry [15]–[18]. Furthermore, the analysis in [14] overlooks the probability of empty cells, in which APs are idle and hence do not act as the source of interference. This is especially evident in underloaded networks as well as general networks that use an AP sleep strategy.

Stochastic geometry has been widely used in cellular networks for modeling the locations of base stations (BSs) as a point process, usually a Poisson point process (PPP) [16] due to its mathematical tractability. Recent advances and results on stochastic geometry modeling of heterogeneous cellular networks can be found in a recent survey [18] and the rich references therein. Due to many fundamental differences between RF communication and VLC [3], existing results obtained for RF-based cellular networks can not be directly applied to VLC networks. Among many significant differences between RF and VLC, a noticeable one is their channel characteristics. More specifically, because the wavelength of visible light is hundreds of nanometers and the detection area of a typical VLC receiver, for example, a photodiode (PD), is millions of square wavelengths. This spatial diversity essentially prevents the "multipath fading" effect in VLC, which in turn makes the calculation of the density function of the SINR more challenging. Furthermore, in cellular networks, the vertical distance of the communication link is generally much smaller than the horizontal distance. Therefore, a planar system model is typically used. However, the size of attocells in VLC networks is in the order of meters. As a result, a three-dimensional system model considering both horizontal and vertical distances of the communication link is required in VLC networks.

B. Contributions

The contributions of this paper are summarized as follows.

1) We consider a three-dimensional attocell model and introduce an analytical framework for the coverage probability analysis in multiuser VLC networks. Based on the user-centric cell association, the proposed framework takes into account the idle probability of APs that are not associated with any users. Specifically, the analytical results are derived as a function of the user density, which is implicitly assumed to be infinity in the existing works [13], [14].
2) By assuming that the point process for the active APs in the network is a thinned homogeneous PPP, we derive an asymptotic result for the coverage probability in the low SINR regime. With the statistical-equivalent transformation, the exact coverage probability in the high SINR regime is derived and given in a mathematically tractable form. A simple and closed-form upper bound on the coverage probability is also provided. The coverage performance is evaluated in detail with various network parameters. We find that the homogeneous PPP assumption for modeling the location of active APs is generally valid, and it gives close results to the exact ones when the density of users is no less than the density of APs.
3) We investigate the effect of receiver noise on the network coverage performance. It is shown that, with typical receiver noise levels (~ -117.0 dBm), the SINR can be well approximated by the signal-to-interference ratio (SIR) for the performance analysis.

C. Paper Organization

The remainder of this paper is organized as follows. Section II describes the three-dimensional attocell model and formulates the SINR metric. With user-centric cell association, the idle probability of APs is derived in Section III. By assuming that the point process of active APs is a homogeneous PPP, analytical expressions for the coverage probability are derived in Section IV. In Section V, we provide numerical examples to validate the derived results and discuss the impact of various network parameters and assumptions on the coverage performance. Finally, Section VI gives the concluding remarks.

II. System Model

We consider a downlink transmission scenario in a multiuser VLC network, with full-frequency reuse, over a three-dimensional indoor space, as depicted in Fig. 1. The VLC APs are vertically fixed since they are attached to the room ceiling while their horizontal locations are modeled by a two-dimensional homogeneous PPP $\Phi_{\mathrm{a}} = \{x_i, i \in \mathbb{N}\} \subset \mathbb{R}^2$, with node density λ_{a}, where x_i is the horizontal distance between AP i and the origin.[1] Similarly, mobile users are also assumed to be at a fixed height, for example, at the desktop level, and

[1]We define the room center as the origin and use both notions interchangeably throughout the paper since the room center has more geographical meanings while the origin has more mathematical meanings in the theoretical analysis.

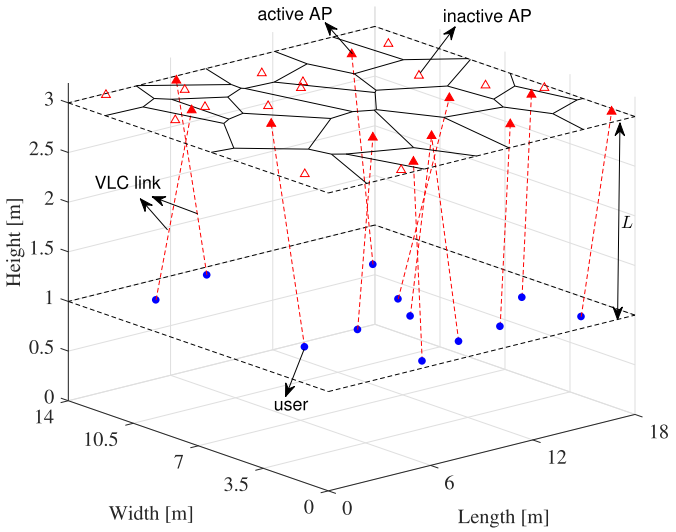

Fig. 1. Three-dimensional Voronoi cell formation in the VLC network assuming the nearest AP association: APs are randomly distributed in the ceiling following Φ_a, while users are randomly distributed at a lower horizontal plane following Φ_u. For the nearest AP association, each user is assumed to be served by the nearest AP in its vicinity.

their horizontal locations are modeled by another independent two-dimensional homogeneous PPP $\Phi_u = \{y_j, j \in \mathbb{N}\} \subset \mathbb{R}^2$, with node density λ_u, where y_j is the horizontal distance between user j and the origin. The vertical separation between Φ_a and Φ_u is denoted by L. After adding an additional user at the room center, the new point process for mobile users becomes $\Phi_u \cup \{0\}$. According to Slivnyak's theorem, adding a user into Φ_u is equivalent to conditioning Φ_u on the added point, and this does not change the distribution of original process Φ_u [15]. The homogeneity and motion-invariant property of the PPP [15] allow us to focus on a *typical* user located at an arbitrary location, and the obtained result would remain the same since it represents the average performance of all users in the network. This is true for an infinite network. For a finite network, the obtained result also remains unchanged, as long as the typical user is far away from room boundaries. This is justified by the power scaling law, stating that the received power is inversely proportional to the link distance and therefore quickly diminishes as the interfering AP is moved further away from the receiver. The origin is usually selected for the location of the typical user due to its notational simplicity. Therefore, in the following analysis, we focused on a typical user located at the origin and discuss the effect of room boundaries in detail in Section V. Note that in a practical VLC network, not all of the APs transmit signals at the same time. Hence, APs that are not in the "communication" mode can either be turned off or operate in the "illumination" mode only, and therefore they do not act as the source of interference in the network. As a result, from the communication perspective, the actual point process of active APs is no longer the same as Φ_a and can be determined by thinning PPP Φ_a to a new process $\tilde{\Phi}_a$.

The complete VLC channel between an AP and a user includes both the line-of-sight (LOS) link and non-line-of-sight (NLOS) links, that are caused by light reflections of interior surfaces in the indoor environment. However, in a typical indoor environment, the signal power of NLOS components is significantly lower than that of the LOS link [1], [2], [6]. Therefore, we will only focus on the LOS link in the following analysis in order to obtain analytically tractable results and insights. Without loss of generality, the VLC AP is assumed to follow the Lambertian radiation profile, whose order can be calculated from $m = -1/\log_2(\cos(\Psi_{1/2}))$, where $\Psi_{1/2}$ denotes the semi-angle of the LED. The PD equipped at each user is assumed to be facing vertically upwards with a field-of-view (FOV) of Ψ_{fov}. For each VLC link, the direct current (DC) gain of the channel is given by [19]:

$$h = \frac{(m+1)A_{pd}\eta}{2\pi d^2}\cos^m(\theta_{tx})G_f(\theta_{rx})G_c(\theta_{rx})\cos(\theta_{rx}), \quad (1)$$

where d is the Euclidean distance between the transmitter and receiver; A_{pd} denotes the effective detection area of the PD; η is the average responsivity of the PD in the white region; θ_{tx} and θ_{rx} are the angle of irradiance and the angle of incidence of the link, respectively; $G_f(\theta_{rx})$ represents the gain of the blue optical filter used at the receiver front end in order to obtain an improved modulation bandwidth; and $G_c(\theta_{rx})$ represents the gain of the optical concentrator, given by [19]:

$$G_c(\theta_{rx}) = \begin{cases} \dfrac{n_c^2}{\sin^2(\Psi_{fov})}, & 0 \le \theta_{rx} \le \Psi_{fov} \\ 0, & \theta_{rx} > \Psi_{fov}, \end{cases} \quad (2)$$

where n_c is the reflective index of the optical concentrator, and it is defined as the ratio of the speed of light in vacuum and the phase velocity of light in the optical material. For visible light, typical values for n_c vary between 1 and 2.

Based on the geometric property [20] of the VLC link, we can obtain $d_i = \sqrt{x_i^2 + L^2}$, $\cos(\theta_{tx,i}) = L/\sqrt{x_i^2 + L^2}$ and $\cos(\theta_{rx,i}) = L/\sqrt{x_i^2 + L^2}$. As a result, the VLC channel gain from AP i to the typical user can be simplified to:

$$h_i(x_i) = \alpha(x_i^2 + L^2)^{-\frac{m+3}{2}}, \quad (3)$$

where $\alpha = (m+1)A_{pd}\eta G_f(\theta_{rx,i})G_c(\theta_{rx,i})L^{m+1}/2\pi$. Denote by x^* the serving AP that gives the highest channel gain to the typical user. We can write

$$x^* = \arg\max_{x_i \in \Phi_a} h_i(x_i) = x_0, \quad (4)$$

where x_0 is the nearest AP in Φ_a to the origin. It can be seen from (4) that the highest channel gain association is equivalent to the nearest AP association, resulting in coverage areas that form the Voronoi tessellation, as depicted in Fig. 1. Therefore, the thinned point process for active APs can be written as:

$$\tilde{\Phi}_a = \left\{\tilde{x}_i, \tilde{x}_i = \arg\min_{x_i \in \Phi_a} ||x_i - y_j||^2, \forall y_j \in \Phi_u\right\}. \quad (5)$$

Direct current biased orthogonal frequency division multiplexing (DCO-OFDM) is assumed as the modulation format, in which the illumination provided by the LED depends on the DC bias, not on the optical signal. Therefore, idle (inactive) APs are the ones that do not transmit optical signals, but they can be either on (DC bias only) or off, depending on the

illumination requirement. Assume that all active APs transmit with the same signal power, that is P_{tx}. Before VLC signal transmission, the optical signal is clipped at both bottom and upper levels to fit into the linear dynamic range of typical LEDs. To facilitate quantifying the effect of clipping distortion, a parameter ξ is introduced, and it is defined as $\xi = P_{\text{opt}}/\sqrt{P_{\text{tx}}}$, where P_{opt}, set by the DC bias, is the required optical power to meet the illumination requirement. According to the three-sigma rule of thumb, $\xi \geq 3$ ensures that at least 99.7% of the optical signal remains unclipped [21]. To make the analysis tractable and, more importantly, to obtained higher SINR of the communication link, we assume in the paper that the signal power satisfies $P_{\text{tx}} \leq P_{\text{opt}}^2/9$ so that the effect of clipping distortion is negligible. Focusing on the typical user, its received interference power is the sum of received powers from all other active APs other than its serving AP. Also, we assume that there is no intra-cell interference, for example, due to the use of orthogonal multiuser access schemes within each Voronoi cell. Therefore, the SINR at the typical user is given by:

$$\mathsf{SINR} = \frac{P_{\text{tx}}\alpha^2(x_0^2 + L^2)^{-(m+3)}}{\sum\limits_{x_i \in \tilde{\Phi}_{\text{a}} \setminus \{x_0\}} P_{\text{tx}}\alpha^2(x_i^2 + L^2)^{-(m+3)} + \sigma^2}, \tag{6}$$

where σ^2 is the receiver noise power including both shot noise and thermal noise. For such small-scaled VLC networks, user performance is typically limited by the interference cause by neighboring APs rather than the noise process at the receiver end. In this case, the SINR can be well approximated by the SIR:

$$\mathsf{SIR} = \frac{(x_0^2 + L^2)^{-(m+3)}}{\sum\limits_{x_i \in \tilde{\Phi}_{\text{a}} \setminus \{x_0\}} (x_i^2 + L^2)^{-(m+3)}}. \tag{7}$$

The goal of this paper is to evaluate the coverage probability of a typical user in the network, which is equivalent to evaluating the complementary cumulative distribution function (CCDF) of the SINR (or SIR in the interference-limited case). The major difficulty resides in characterizing $\tilde{\Phi}_{\text{a}}$ because the probability density function (PDF) of the Voronoi cell in PPP still remains unknown [15], [22]–[24]. With this in mind, we simplify the problem by making the following assumption.

Assumption 1: The point process for active APs, $\tilde{\Phi}_{\text{a}}$, is a homogeneous PPP, whose intensity is given by $\tilde{\lambda}_{\text{a}} = (1 - p_{\text{idle}})\lambda_{\text{a}}$, where p_{idle} represents the idle probability of APs in the network that are not associated with any users.

In the following, we calculate the idle probability of APs in Section III. In Section IV, we derive analytical results for the coverage probability based on Assumption 1. The accuracy of the obtained results built upon this assumption is later justified in Section V.

III. Idle Probability of APs

Consider a Voronoi cell $\mathcal{A} \subset \mathbb{R}^2$ generated from PPP Φ_{a}. We are interested in finding the probability that there exist k users inside $\mathcal{A}$:

$$\mathbb{P}\left[\sum_{y_i \in \Phi_{\text{u}}} \mathbf{1}_{\mathcal{A}}(y_i) = k\right] = \mathbb{E}_{\mathcal{A}}\left[\frac{(\lambda_{\text{u}}\mu(\mathcal{A}))^k}{k!}\exp\left(-\lambda_{\text{u}}\mu(\mathcal{A})\right)\right], \tag{8}$$

where $\mu(\mathcal{A})$ is the standard Lebesgue measure of $\mathcal{A}$, and $\mathbf{1}_{\mathcal{A}}(y_i)$ is the random counting measure of $\mathcal{A}$, defined as:

$$\mathbf{1}_{\mathcal{A}}(y_i) = \begin{cases} 1, & y_i \in \mathcal{A} \\ 0, & \text{otherwise} \end{cases}. \tag{9}$$

Although the exact PDF of $\mu(\mathcal{A})$ is unknown, existing studies have reported that it can be well approximated with a Gamma distribution $\mu(\mathcal{A}) \sim \text{Gamma}(\beta, \beta\lambda_{\text{a}})$, whose PDF is given by [22]:

$$f_{\mu(\mathcal{A})}(t) = \frac{(\beta\lambda_{\text{a}})^\beta}{\Gamma(\beta)} t^{\beta-1}\exp\left(-\beta\lambda_{\text{a}}t\right), \tag{10}$$

where $\Gamma(\cdot)$ is the gamma function, and the shape parameter $\beta = 3.5$ [22] is obtain through curve fitting. With this approximated PDF, (8) can be calculated as:

$$\begin{aligned}\mathbb{P}\left[\sum_{y_i \in \Phi_{\text{u}}} \mathbf{1}_{\mathcal{A}}(y_i) = k\right] &= \int_0^\infty \frac{(\lambda_{\text{u}}t))^k}{k!}\exp\left(-\lambda_{\text{u}}t\right) f_{\mu(\mathcal{A})}(t)\mathrm{d}t \\ &= \frac{1}{k!}\frac{\Gamma(\beta+k)}{\Gamma(\beta)}\left(\frac{\beta}{\beta+\frac{\lambda_{\text{u}}}{\lambda_{\text{a}}}}\right)^\beta\left(\frac{\frac{\lambda_{\text{u}}}{\lambda_{\text{a}}}}{\beta+\frac{\lambda_{\text{u}}}{\lambda_{\text{a}}}}\right)^k. \end{aligned} \tag{11}$$

The idle probability of APs can be obtained by plugging $k = 0$ into (11), yielding:

$$p_{\text{idle}} = \mathbb{P}\left[\sum_{y_i \in \Phi_{\text{u}}} \mathbf{1}_{\mathcal{A}}(y_i) = 0\right] = \left(\frac{\beta}{\beta + \frac{\lambda_{\text{u}}}{\lambda_{\text{a}}}}\right)^\beta. \tag{12}$$

It can be seen from (12) that the idle probability of APs is determined by the ratio of user density to AP density, but not the exact value of user density or AP density.

Remark 1: By applying Jensen's inequality, the idle probability of APs is lower bounded by $\exp(-\lambda_{\text{u}}/\lambda_{\text{a}})$. This result follows from $p_{\text{idle}} = \mathbb{E}_{\mathcal{A}}[\exp(-\lambda_{\text{u}}\mu(\mathcal{A}))] \geq \exp\left(-\lambda_{\text{u}}\mathbb{E}_{\mathcal{A}}[\mu(\mathcal{A})]\right)$ and $\mathbb{E}_{\mathcal{A}}[\mu(\mathcal{A})] = \lambda_{\text{a}}^{-1}$.

IV. Coverage Probability Analysis

In this section, we focus on the analysis of the coverage probability of a typical user in the network. Since the distribution function of the SINR exhibits different behaviors at low and high values, we separate the analysis into two regimes: 1) in the low SINR regime, where the SINR target is smaller than one. 2) in the high SINR regime, where the SINR target is larger than one.

A. Asymptotic Analysis of the Coverage Probability in the Low SINR Regime

Assumption 2: The multiuser VLC network under consideration is interference-limited so that the SINR can be well approximated by the SIR.

Remark 2: Assumption 2 plays an important role in simplifying the analysis of the coverage probability in Section IV-A. The validation of Assumption 2 is later justified in Section V through simulation results. However, note that Assumption 2 is not explicitly made when we evaluate the coverage probability in the high SINR regime in Section IV-B.

With Assumption 2, we first study the distribution of the interference-to-signal ratio (ISR) at the typical user, given by $\mathsf{ISR} = \mathsf{SIR}^{-1}$. The Laplace transform of the ISR is given in the following theorem.

Theorem 1: The Laplace transform of the ISR of a typical user is given by:

$$\mathcal{L}_{\mathsf{ISR}}(s) = \frac{1}{\frac{1}{m+3}E_{\frac{m+4}{m+3}}(s) + \Gamma\left(\frac{m+2}{m+3}\right)s^{\frac{1}{m+3}}} \exp\Bigg[-\pi\tilde{\lambda}_{\mathrm{a}}L^2 \times \left(-1 + \frac{1}{m+3}E_{\frac{m+4}{m+3}}(s) + \Gamma\left(\frac{m+2}{m+3}\right)s^{\frac{1}{m+3}}\right)\Bigg], \tag{13}$$

where $E_n(z) = \int_1^\infty \exp(-zt)t^{-n}\mathrm{d}t$ is the exponential integral function [25].

Proof: Please refer to Appendix A. ∎

The denominator of the Laplace transform of the ISR is a strictly increasing function with respect to s because its first order derivative is positive:

$$\frac{\partial(1+W(s))}{\partial s} = -\frac{1}{m+3}E_{\frac{1}{m+3}}(s) + \frac{1}{m+3}\Gamma\left(\frac{m+2}{m+3}\right)s^{-\frac{m+2}{m+3}} > 0, \tag{14}$$

in which function $W(s)$ is defined in (32). Furthermore, the denominator of $\mathcal{L}_{\mathsf{ISR}}(s)$ also satisfies $1+W(0) = 1$. Hence, it is shown that the denominator of the Laplace transform of the ISR has only a single root s^* so that $1 + W(s^*) = 0$. The region of convergence (ROC) of the Laplace transform of the ISR is therefore $\Re(s) > \Re(s^*)$, where $\Re(s)$ denotes the real part of s. From (32), it can be seen that the denominator of the Laplace transform is dependent on the Lambertian order of the AP. In other words, the pole of Laplace transform of ISR changes as the Lambertian order of the AP changes. Although a symbolic expression for s^* is not available, its numerical value can be efficiently calculated using standard mathematical software packages. In Fig. 2, the denominator of $\mathcal{L}_{\mathsf{ISR}}(s)$ is plotted against different values of s. It is verified that the denominator of the Laplace transform is a strictly increasing function of s, and it has a single root on the negative real axis. The numerical value of the pole of $\mathcal{L}_{\mathsf{ISR}}(s)$ is found to be -2.173, -1.847 and -1.658 when the semi-angle of the AP is set to 45°, 60° and 75°, respectively.

From the Laplace transform, the coverage probability of a typical user can be obtained by means of the inverse Laplace transform as follows:

$$\mathbb{P}\left[\mathsf{ISR} > T\right] = 1 - \mathcal{L}^{-1}\left\{\frac{\mathcal{L}_{\mathsf{ISR}}(s)}{s}\right\}(\mathsf{ISR})\Big|_{\mathsf{ISR}=T}. \tag{15}$$

Since $\mathcal{L}_{\mathsf{ISR}}(s)/s$ is a nonstandard Laplace function, the exact expression of its inverse, and hence the coverage probability, is hard to obtain. However, its asymptotic property can be utilized to calculate the coverage probability in the low SIR regime. This is stated in the following corollary.

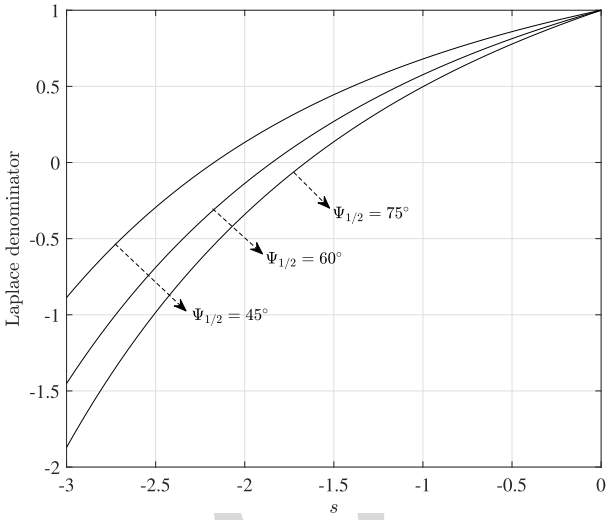

Fig. 2. The denominator of the Laplace transform of the ISR as a function of s.

Corollary 1: The coverage probability of a typical user in the low SIR regime, i.e., $T < 1$, can be approximated by:

$$\mathbb{P}\left[\mathsf{SIR} > T\right] \approx 1 - \exp\left(\frac{s^*}{T}\right), \tag{16}$$

in which s^* is the pole of the Laplace transform of the ISR given in (13).

Proof: The coverage probability can be rewritten as $\mathbb{P}\left[\mathsf{SIR} > T\right] = \mathbb{P}\left[\mathsf{ISR} < 1/T\right]$. Since s^* is a pole of $\mathcal{L}_{\mathsf{ISR}}(s)$, and the abscissa of convergence of the Laplace transform is negative finite, we have the following result from [26]:

$$\lim_{T\to 0^+} T\log\left(\mathbb{P}\left[\mathsf{ISR} > \frac{1}{T}\right]\right) = s^*. \tag{17}$$

For small values of the ISR, (16) can be obtained by rewriting the result in (17). ∎

Remark 3: The pole of the Laplace transform of the ISR does not depend on the parameter L, and therefore the coverage probability of the typical user does not depend on L.

The exponential approximation of the coverage probability in (16) is only valid in the low SIR regime. When $T > 1$, new results for the coverage probability are derived in Section IV-B.

B. Analysis of the Coverage Probability in the High SINR Regime

In this subsection, we focus on evaluating the coverage probability in the high SINR regime. Different from the analysis presented in Section IV-A, here we present more general and exact analysis on the coverage probability by considering both interference and noise in the system model. The derived result complements the result presented in Section IV-A in that it applies to the computation of the coverage probability when $T > 1$, which is a more realistic scenario for practical VLC systems.

From (6), the SINR of a typical user can be simplified to:

$$\mathsf{SINR} = \frac{(x_0^2 + L^2)^{-(m+3)}}{\sum\limits_{x_i \in \tilde{\Phi}_\mathrm{a} \setminus \{x_0\}} (x_i^2 + L^2)^{-(m+3)} + \bar{\sigma}^2}, \tag{18}$$

where the noise power has been normalized to $\bar{\sigma}^2 = \sigma^2 / P_{\mathrm{tx}} \alpha^2$.

Definition 1: Consider two stochastic point processes Φ_1 and Φ_2 for modeling horizontal locations of APs in the VLC network. The SINR models used for Φ_1 and Φ_2 are SINR_1 and SINR_2, respectively. Φ_1 (with SINR_1) is said to be *statistically equivalent* [27] to Φ_2 (with SINR_2) if the distribution of the SINR at the typical user is the same for Φ_1 and Φ_2, i.e., $\mathbb{P}[\mathsf{SINR}_1 > T] = \mathbb{P}[\mathsf{SINR}_2 > T]$. Mathematically, we denote $\Phi_1 \overset{\text{s.e.}}{=} \Phi_2$ and $\mathsf{SINR}_1 \overset{\text{s.e.}}{=} \mathsf{SINR}_2$.

Remark 4: For $\Phi_1 \overset{\text{s.e.}}{=} \Phi_2$, it is sufficient but not necessary that $\Phi_1 = \Phi_2$. However, for $\Phi_1 = \Phi_2$, it is necessary but not sufficient that $\Phi_1 \overset{\text{s.e.}}{=} \Phi_2$.

Since the evaluation of the coverage probability is not straightforward with $\tilde{\Phi}_\mathrm{a}$ and the SINR model given in (18), with Definition 1, we can now focus on analyzing another point process with a more tractable SINR model, as long as both point processes are statistically equivalent.

Theorem 2: The two-dimensional homogeneous PPP $\tilde{\Phi}_\mathrm{a}$, with density $\tilde{\lambda}_\mathrm{a}$ and the SINR model given in (18), is statistically equivalent to another one-dimensional point process $\tilde{\Phi}_{\mathrm{eq}}$, whose density function is:

$$\tilde{\lambda}_{\mathrm{eq}}(x) = \frac{\pi \tilde{\lambda}_\mathrm{a}}{\Gamma\left(\frac{1}{m+3}\right)} x^{\frac{1}{m+3}-1}, \tag{19}$$

for $x > L^{2(m+3)}$, and zero otherwise. The equivalent SINR model for $\tilde{\Phi}_{\mathrm{eq}}$ is:

$$\mathsf{SINR}_{\mathrm{eq}} = \frac{g_0 x_0^{-1}}{\sum\limits_{x_i \in \tilde{\Phi}_{\mathrm{eq}} \setminus \{x_0\}} g_i x_i^{-1} + \bar{\sigma}^2}, \tag{20}$$

where g_i, $i = 0, 1, \cdots$, are auxiliary random variables that are exponentially distributed with unity mean, i.e., $g_i \sim \exp(1)$.

Proof: Please refer to Appendix B. ∎

Remark 5: For the original SINR model given in (18), x_i, for $i = 0, 1, \cdots$, takes values between interval $[0, \infty]$. However, for the equivalent SINR model given in (20), x_i, for $i = 0, 1, \cdots$, takes values between interval $\left[L^{2(m+3)}, \infty\right]$. This should be treated carefully when using the density function (19).

Remark 6: Other distributions can also be assumed for auxiliary random variables g_i. However, this requires a recalculation of the density function $\tilde{\lambda}_{\mathrm{eq}}(x)$ in order to maintain the statistical equivalence.

Although Theorem 2 transforms the original homogeneous two-dimensional PPP $\tilde{\Phi}_\mathrm{a}$ into an inhomogeneous PPP $\tilde{\Phi}_{\mathrm{eq}}$, it also transforms the original SINR expression in (18) with a Euclidean distance path-loss model into a new SINR expression in (20) with a planar distance path-loss model, multiplied by auxiliary random variables g_i, which mimics the small-scale fading effect in RF based cellular networks. It will be shown in the following analysis that this statistical-equivalent transformation can significantly simplify the calculation of the coverage probability in VLC networks. Specifically, with exponentially distributed auxiliary random variables g_i, the calculation of the coverage probability can now be expressed as a function of exponential terms, which was not possible for the no-fading case in (18).

Based on the statistical-equivalent SINR model given in (20), we have the following result for the coverage probability of a typical user in the network.

Theorem 3: When the SINR target is greater than one, i.e., $T > 1$, the coverage probability of a typical user in the network is given by:

$$\begin{aligned}\mathbb{P}\left[\mathsf{SINR} > T\right] = \int_{L^{2(m+3)}}^{\infty} & \frac{\pi \tilde{\lambda}_\mathrm{a}}{\Gamma\left(\frac{1}{m+3}\right)} x^{\frac{1}{m+3}-1} \exp\left(-T\bar{\sigma}^2 x\right) \\ & \times \exp\left[-\frac{\pi \tilde{\lambda}_\mathrm{a}}{m+2} \frac{L^{-2(m+2)}}{\Gamma\left(\frac{m+4}{m+3}\right)} T x \right. \\ & \left. \times {}_2F_1\left(1, \frac{m+2}{m+3}; \frac{2m+5}{m+3}; -L^{-2(m+3)} T x\right)\right] \mathrm{d}x, \end{aligned} \tag{21}$$

where ${}_2F_1(\cdot, \cdot; \cdot; \cdot)$ denotes the Gauss hypergeometric function [25].

Proof: Please refer to Appendix C. ∎

When the SINR threshold does not satisfy $T > 1$, (21) does not hold because $\mathbb{P}[\mathsf{SINR} > T] < \sum_{i=0}^{\infty} \mathbb{P}[\mathsf{SINR}_i > T]$. In this case, the analytical expression derived in (21) serves as an upper bound on the coverage probability of a typical user. Due to the involved Gauss hypergeometric function, a closed-form expression for the coverage probability is not available. However, the coverage probability can still be computed using numerical methods. In Appendix D, we provide a numerical method for efficient computation of (21).

Remark 7: When $L = 0$, (21) can not be applied. However, in this case, Theorem 3 still holds, and the coverage probability of a typical user can be calculated by $\lim_{L \to 0} \mathbb{P}[\mathsf{SINR} > T]$.

In fact, when $L = 0$, another simpler expression for the coverage probability is available:

$$\begin{aligned}\mathbb{P}\left[\mathsf{SINR} > T\right] = \int_{0}^{\infty} & \frac{\pi \tilde{\lambda}_\mathrm{a}}{\Gamma\left(\frac{1}{m+3}\right)} x^{\frac{1}{m+3}-1} \exp\left(-T\bar{\sigma}^2 x\right) \\ & \times \exp\left[-\pi \tilde{\lambda}_\mathrm{a} \Gamma\left(\frac{m+2}{m+3}\right) (Tx)^{\frac{1}{m+3}}\right] \mathrm{d}x. \end{aligned} \tag{22}$$

Furthermore, significant simplification is possible for the interference-limit case, i.e., when $\bar{\sigma}^2 = 0$. The simplified result for this case is given in the following corollary.

Corollary 2: When $L = 0$, the coverage probability in the interference-limited scenario follows a power-law decay profile:

$$\mathbb{P}\left[\mathsf{SINR} > T\right] = \frac{1}{\Gamma\left(\frac{m+2}{m+3}\right) \Gamma\left(\frac{m+4}{m+3}\right)} T^{-\frac{1}{m+3}}. \tag{23}$$

Proof: This result follows directly from (22) after setting $\bar{\sigma}^2 = 0$. ∎

C. An Upper Bound on the Coverage Probability

Considering the SINR model given in (18), the coverage probability of a typical user can also be calculated in a brute-force way:

$$\mathbb{P}\left[\mathsf{SINR} > T\right] = \int \cdots \int_{D(T)} f_{x_0,x_1,\cdots,x_n}(x_0, x_1, \cdots, x_n)\mathrm{d}x_0\mathrm{d}x_1\cdots\mathrm{d}x_n, \tag{24}$$

where $D(T)$, as a function of the SINR target T, is the domain of integration formed by the $n+1$ variables according to the inequality $\mathsf{SINR} > T$, and $f_{x_0,x_1,\cdots,x_n}(x_0, x_1, \cdots, x_n)$ is the joint distance distribution of the nearest $n+1$ APs in the PPP [28]. Since the domain of integration is highly coupled by $x_0, x_1, \cdots, x_n$, it is typically hard to compute the coverage probability directly with (24). To simplify the problem, we consider only the serving AP x_0 and the nearest interfering AP to the typical user, i.e., x_1. The obtained result therefore serves as an upper bound on the coverage probability since it ignores the effect of receiver noise and underestimates the interference level and hence overestimates the SINR. This result is stated in the following proposition.

Proposition 1: An upper bound on the coverage probability of a typical user is:

$$\mathbb{P}\left[\mathsf{SINR} > T\right] \leq T^{-\frac{1}{m+3}} \exp\left(-\pi\tilde{\lambda}_{\mathrm{a}}L^2\left(T^{\frac{1}{m+3}}-1\right)\right). \tag{25}$$

Proof: Based on the SINR expression given in (18), we have $\mathsf{SINR} \leq (x_0^2+L^2)^{-(m+3)}/(x_1^2+L^2)^{-(m+3)}$ after ignoring the power of interference generated from $\tilde{\Phi}_{\mathrm{a}}\backslash\{x_0, x_1\}$. It immediately follows that $\mathbb{P}[\mathsf{SINR} > T] \leq \mathbb{P}\left[(x_0^2+L^2)^{-(m+3)}/(x_1^2+L^2)^{-(m+3)} > T\right] = \mathbb{P}\left[x_1 > \sqrt{T^{\frac{1}{m+3}}(x_0^2+L^2)-L^2}\right]$. Given that the joint PDF of x_0 and x_1 is $f_{x_0,x_1}(x_0, x_1) = \exp(-\pi\tilde{\lambda}_{\mathrm{a}}x_1^2)(2\pi\tilde{\lambda}_{\mathrm{a}})^2x_0x_1$ [28], we have:

$$\mathbb{P}\left[x_1 > \sqrt{T^{\frac{1}{m+3}}(x_0^2+L^2)-L^2}\right] = \int_0^{\infty}\int_{\sqrt{T^{\frac{1}{m+3}}(x_0^2+L^2)-L^2}}^{\infty} f_{x_0,x_1}(x_0, x_1)\mathrm{d}x_1\mathrm{d}x_0. \tag{26}$$

Calculating the double integral in (26) yields the upper bound expression given in (25). ■

Remark 8: The derivation of this upper bound does not necessarily require $T > 1$. However, it is not meaningful to apply this upper bound to low SINR regimes since for $T \leq 1$ it is definite that $T^{-\frac{1}{m+3}} \exp\left(-\pi\tilde{\lambda}_{\mathrm{a}}L^2\left(T^{\frac{1}{m+3}}-1\right)\right) \geq 1$.

V. Simulation Results and Discussions

Monte Carlo simulation results are presented in this section to validate the theoretical results derived in the previous section. The impacts of previously made assumptions on the accuracy of the results are also discussed. An indoor office of size $18\times14\times3.5$ m^3 is considered, as depicted in Fig. 1. If not otherwise specified, the following parameters are used for the simulation setup. The VLC APs have a semi-angle of 60°, and all active APs transmit at the same power level, that is 1 W.

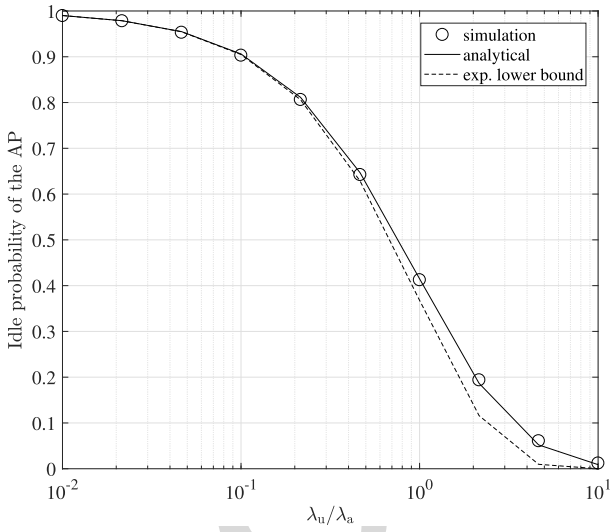

Fig. 3. Idle probability of the AP in the VLC network. $\lambda_{\mathrm{a}} = 0.1$.

The PD used at the receiver side has 90° FOV, an effective detection area of 1 cm^2, and a responsivity of 0.4 A/W. Despite the bandwidth limitation of commercially available white LEDs, current works have shown that using a blue optical filter at the receiver front end can achieve an increased modulation bandwidth of up to 20 MHz [29], [30]. Therefore, a modulation bandwidth of 20 MHz and a noise power spectral density of 10^{-22} A^2/Hz (after blue filtering) [1], [2], [6] is assumed in the simulation. The typical value of the receiver noise power is therefore -117.0 dBm. At the receiver front end, the optical concentrator has a reflective index of 1.5, and the optical filter has a unity gain.

First, based on the highest channel gain association, the idle probability of APs in a typical Voronoi cell is evaluated and the results are shown in Fig. 3. The procedure of calculating the idle probability of the AP using Monte Carlo simulations can be summarized as follows. First, based on the PPP model, generate one realization of independent random locations of APs and users. Second, for each random user, find the AP that gives the highest channel gain based on (4). If, on rare occasions, there are multiple solutions to (4), choose one of the optimal APs randomly. Third, after all users have connected to their optimal APs, count the number of APs that are not connected to any user. The idle probability is therefore calculated as the ratio between the number of unconnected APs and the total number of APs. Finally, generate a large number of realizations, and then calculate the average of the idle probability. It can be seen that analytical results agree well with simulation results, and the exponential lower bound on the idle probability is reasonably accurate, especially when $\lambda_{\mathrm{u}}/\lambda_{\mathrm{a}}$ is small. Fig. 3 also shows that, with given simulation parameters, the idle probability of the AP is nonzero unless $\lambda_{\mathrm{u}} > 10\lambda_{\mathrm{a}}$. Specifically, when the density of users in the network is smaller than the density of APs, i.e., $\lambda_{\mathrm{u}}/\lambda_{\mathrm{a}} \leq 1$, the idle probability is above 0.4. For an underloaded network, e.g., $\lambda_{\mathrm{u}}/\lambda_{\mathrm{a}} = 0.1$, the AP idle probability can be as large as 0.9. Therefore, results in Fig. 3 indicate that considering all of the APs in the network as interfering nodes is inaccurate

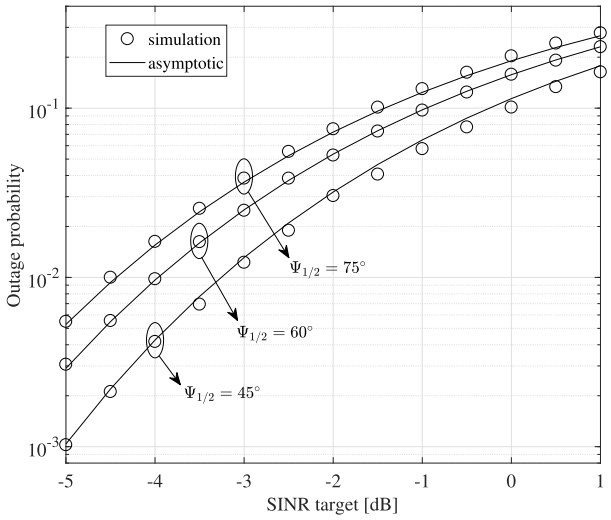

Fig. 4. Outage probability of a typical user in the low SINR regime. $\tilde{\lambda}_{\mathrm{a}} = 0.15$ and $L = 2$ m.

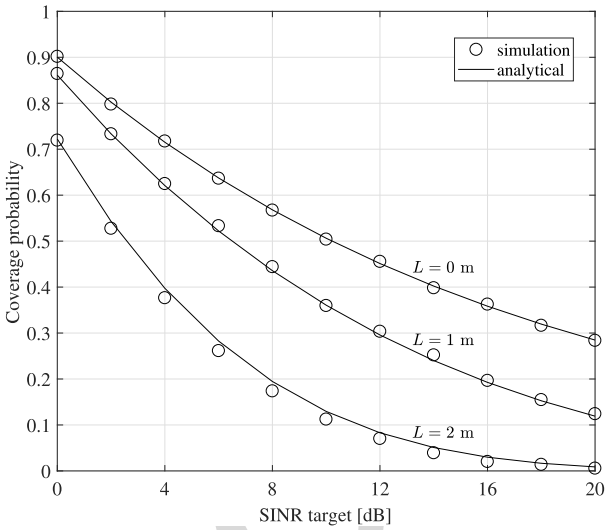

Fig. 5. Coverage probability of a typical user in the high SINR regime. $\tilde{\lambda}_{\mathrm{a}} = 0.1$.

when $\lambda_{\mathrm{u}} < 10\lambda_{\mathrm{a}}$, and this will lead to the underestimation of the coverage performance of users in the network. On the other hand, in an overloaded network where the density of users is about ten times larger than the density of APs, the idle probability of APs can be ignored since its average value approaches zero.

A. Results Based on Assumption 1

In this subsection, we assume that the active APs are a thinned PPP with density $\tilde{\lambda}_{\mathrm{a}} = (1 - p_{\mathrm{idle}})\lambda_{\mathrm{a}}$ (Assumption 1), and discuss the effect of various network parameters on the coverage performance. In Fig. 4, the outage probability[2] of a typical user in the low SINR regime is evaluated. It can be seen that the derived asymptotic expression accurately captures the SINR characteristics when SINR is nearly zero. As the SINR target approaches one, the asymptotic result becomes less accurate. Fig. 4 also shows that using APs with a smaller semi-angle gives better coverage performance at the typical user. This is contradictory to indoor lighting requirements since more uniform illumination would require to install APs with a larger semi-angle. However, this finding is not surprising and can be explained as follows. Although APs with a smaller semi-angle generate more directional light beams, hence less light coverage per AP, they improve the achievable SINR at a typical user because higher signal power and less interference is generated.

Compared to the asymptotic result shown in Fig. 4, the SINR distribution in the high SINR region is typically of more interest. It is shown in Fig. 5 that the derived analytical expression for the coverage probability of a typical user in the high SINR regime is well matched with simulation results. When $L = 0$, the three-dimensional network model reduces to a two-dimensional planar model, and the coverage probability is found to follow a power-law decay profile. When $L \neq 0$, the coverage probability decay is more involved and it does not follow the power law any more. In fact, the decay is shown to be more rapid at the beginning and steady at the tail.

[2]The outage probability is the complement of the coverage probability. We plot outage probability in Fig. 4 because the coverage probability is less distinguishable when the SINR target is low.

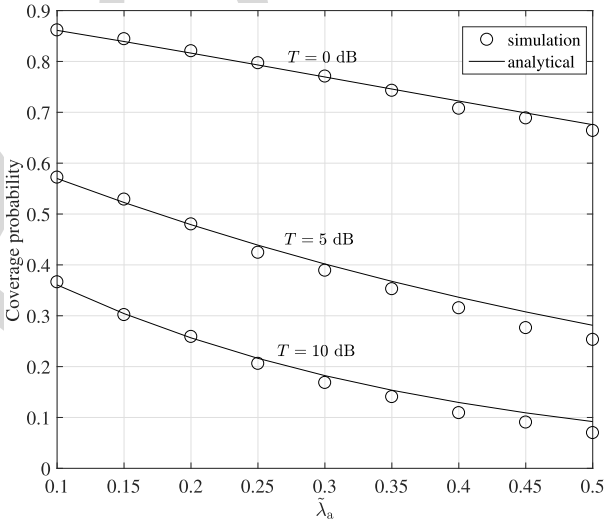

Fig. 6. Coverage probability of a typical user for different densities of the VLC APs. $L = 1$ m.

The impact of the density of APs on the coverage probability of a typical user is evaluated in Fig. 6. As expected, results confirm that, without efficient interference mitigation techniques, the coverage probability reduces as the density of APs increases. This is because that the legitimate user is served by the nearest AP while the increasing number of APs brings an increment of the interference power. However, the decay rate of the coverage probability reduces as the density of active APs increases.

Fig. 7 compares the exact and asymptotic expressions for the coverage probability as a function of parameter L. In general, the coverage probability at a typical user decreases as L increases. The decay of the coverage probability is observed to be steady at small values of L and rapid for large values of L.

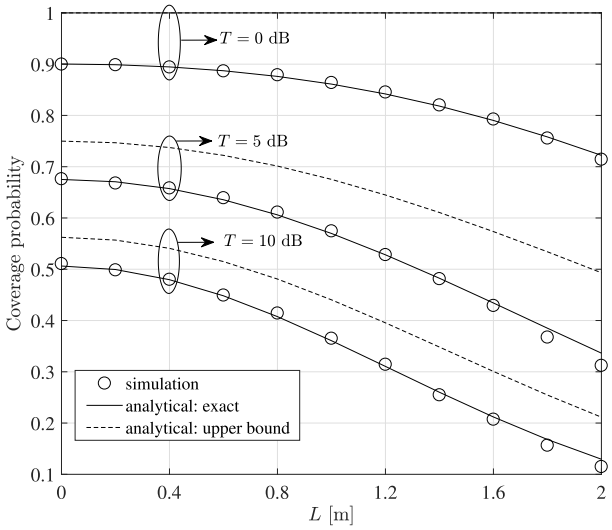

Fig. 7. Coverage probability of a typical user for different values of L. $\tilde{\lambda}_\mathrm{a} = 0.1$.

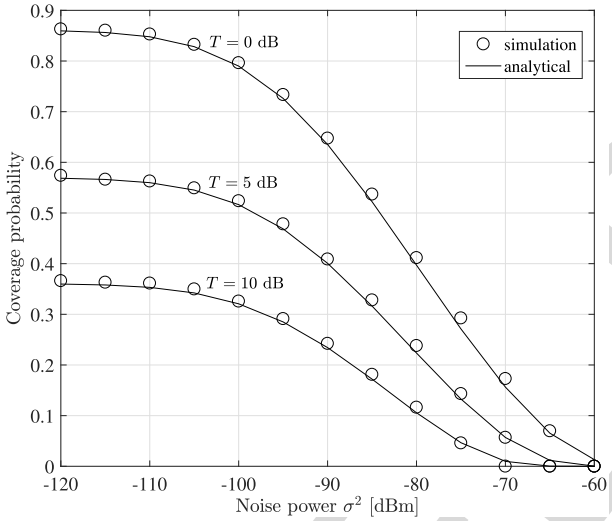

Fig. 8. The impact of noise power on the coverage probability of a typical user. $\tilde{\lambda}_\mathrm{a} = 0.1$ and $L = 1$ m.

The derived analytical expression agrees well with simulation results while the asymptotic expression exhibits a positive gap from the exact one. This gap is caused by underestimating the interference power at the typical user, as stated in Proposition 1. For larger values of T, the gap between the asymptotic result and the exact one becomes tighter. Despite the accuracy of the asymptotic upper bound, it is extremely simple to compute. However, when $T = 0$ dB, this asymptotic upper bound becomes a constant unity bound.

B. Is Assumption 2 Valid?

The asymptotic result shown in Fig. 4 did not consider the effect of receiver noise, but is shown to be reasonably accurate. The analytical results shown in Figs. 5 to 7 did consider the effect of receiver noise, at the cost of being more computationally expensive. So the question is, can the receiver noise be ignored for the coverage analysis in VLC networks (Assumption 2)? To answer this question, in Fig. 8 we evaluate the coverage probability of a typical user with different values of the receiver noise power. It can be seen that, in our simulation setup, the coverage probability is not affected by the receiver noise process, as long as the noise power is below -110 dBm. However, when the power of receiver noise exceeds this threshold, the effect of receiver noise can no longer be ignored, and it starts to deteriorate the coverage performance of a typical user. Fig. 8 also shows that the effect of receiver noise is more dominant when T is small and less dominant when T is large. Nevertheless, the derived analytical result is applicable to the general case with arbitrary noise levels. For typical receiver noise of power -117.0 dBm [1], [6], it is safe to assume that the VLC network is interference-limited, as stated in Assumption 2, and to study the coverage performance using the SIR rather than the SINR.

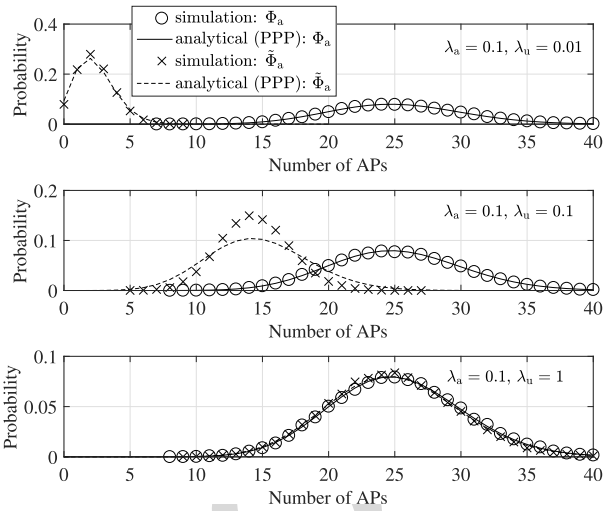

Fig. 9. Probability mass function of Φ_a and $\tilde{\Phi}_\mathrm{a}$.

C. Is Assumption 1 Valid?

In Fig. 3, the derived idle probability of VLC APs is shown to be accurate. However, it does not confirm that the thinned process $\tilde{\Phi}_\mathrm{a}$ is a homogeneous PPP. Therefore, the second question to ask is, is Assumption 1 valid? In order to answer this question, two aspects, namely PPP and homogeneity, need to be studied. In Figs. 9 and 10, we compute the PMF of active APs and compare the exact result with the analytical one (based on Assumption 1). It is shown in Fig. 9 that the number of active APs is not necessarily Poisson-distributed. Specifically, when $\lambda_\mathrm{a} = 0.1$ and $\lambda_\mathrm{u} = 0.01$, the PMF of active APs does follow the Poisson distribution, whose intensity is $\tilde{\lambda}_\mathrm{a} = (1 - p_\mathrm{idle})\lambda_\mathrm{a}$. Mathematically, it is given by:

$$\mathbb{P}\left[\sum_{x_i \in \tilde{\Phi}_\mathrm{a}} \mathbf{1}_{\mathcal{A}}(x_i) = n\right] = \frac{(\tilde{\lambda}_\mathrm{a}\mu(\mathcal{A}))^n}{n!} \exp\left(-\tilde{\lambda}_\mathrm{a}\mu(\mathcal{A})\right), \quad (27)$$

for $n = 0, 1, \cdots$, and zero otherwise. To evaluate the PMF of active APs in the network, $\mathcal{A}$ should be set to the entire (horizontal) area of the indoor environment, so that its standard Lebesgue measure is $\mu(\mathcal{A}) = 18 \times 14$ m^2. The Poisson assumption is also valid when $\lambda_\mathrm{a} = 0.1$ and $\lambda_\mathrm{u} = 1$.

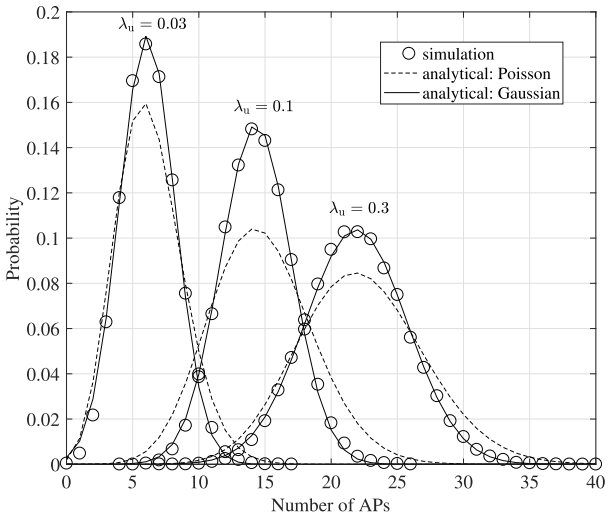

Fig. 10. Gaussian curve fitting for the probability mass function of $\tilde{\Phi}_a$. $\lambda_a = 0.1$.

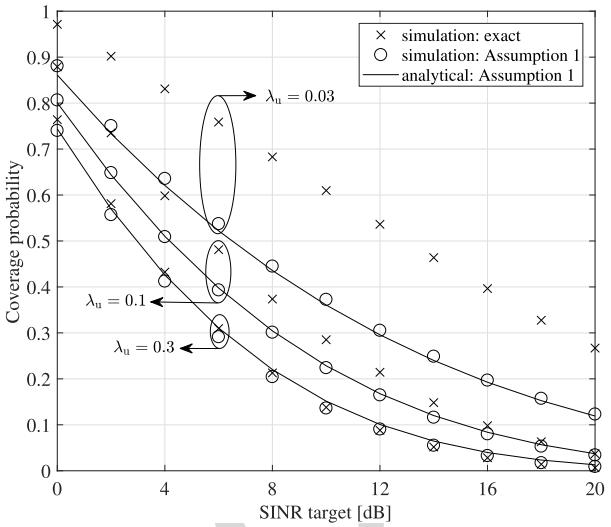

Fig. 11. Coverage probability comparison between the thinned PPP model and the exact results. $\lambda_a = 0.1$ and $L = 2$ m.

TABLE I
GAUSSIAN COEFFICIENTS OBTAINED FROM CURVE FITTING

	a_G	b_G	c_G
$\lambda_u = 0.03$	0.1894	6.093	2.985
$\lambda_u = 0.1$	0.1502	14.32	3.751
$\lambda_u = 0.3$	0.1037	21.89	5.446

In fact, in this case the PMF of active APs is identical to the PMF of all APs in the network since the idle probability is now approximately zero. However, when $\lambda_a = \lambda_u = 0.1$, it is shown that the number of active APs does not follow the PPP anymore, although the actual process and the thinned PPP model have the same mean. Based on these observations, we can conclude from Fig. 9 that the PPP assumption is accurate only when APs and users have distinctive node intensities, or equivalently speaking, when the idle probability of APs is either approximately zero or approximately one. As a rule of thumb, we can say that the PPP assumption is valid when $\lambda_u/\lambda_a \leq 0.1$ or $\lambda_u/\lambda_a \geq 10$, which corresponds to $p_{idle} \geq 0.91$ or $p_{idle} \leq 0.01$, respectively (see Fig. 3).

Fig. 9 has showed that the PMF of active APs doe not follow the PPP when λ_a and λ_u are of similar values. To investigate further, we plot in Fig. 10 the PMF of the active APs when $\lambda_a = 0.1$ and $\lambda_u = 0.03, 0.1, 0.3$. This corresponds to $\lambda_u/\lambda_a = 0.3, 1, 3$, respectively. It can be seen from Fig. 10 that number of active APs can be well modeled by the discrete Gaussian distribution, whose PMF is:

$$\mathbb{P}\left[\sum_{x_i \in \tilde{\Phi}_a} \mathbf{1}_{\mathcal{A}}(x_i) = n\right] = a_G \exp\left(-\left(\frac{n - b_G}{c_G}\right)^2\right), \quad (28)$$

where a_G, b_G, c_G are the coefficients obtained from Gaussian curve fitting, that are related to λ_a, λ_u and also the Lebesgue measure of $\mathcal{A}$. For the considered indoor environment, the fitted Gaussian coefficients are summarized in Table I. Although the exact expressions for coefficients a_G and c_G are still unclear, the expression for coefficient b_G can be approximated by $b_G = (1 - p_{idle})\lambda_a \mu(\mathcal{A})$. This result follows directly from the fact that the Poisson approximation and the Gaussian approximation of the PMF of $\tilde{\Phi}_a$ have the same mean (see Figs. 9 and 10).

To investigate the homogeneity assumption for $\tilde{\Phi}_a$, we show in Fig. 11 the coverage probability of a typical user, comparing the exact result obtained from simulations with the result obtained based on Assumption 1. It is interesting to note that, for a low density of users, the distribution of active APs can be approximated as the PPP, but not a homogeneous one. In fact, a homogeneous PPP assumption will underestimate the coverage probability of a typical user in the network. When the density of users and the density of APs are similar, modeling the active APs in the network as a homogeneous PPP is acceptable since this model only brings small errors to the coverage probability result. When the density of users is larger than the density of APs, for example, in an overloaded network, the homogeneous PPP assumption is found to be very accurate because the idle probability of APs in an overloaded network is approximately zero. Moreover, compared to previous works that do not consider the idleness of APs, e.g., [14], the proposed analytical framework is shown to better capture the characteristics of underloaded networks and certain networks that operate with an AP sleep strategy to save energy and/or minimize the co-channel interference. For overloaded networks, in which the effect of AP idleness can be ignored, the results derived in [14] can also be obtained from the proposed framework by setting λ_u towards infinity.

D. Effect on Room Boundaries

To facilitate analytically tractable derivations, the VLC network is assumed to extend towards infinity, as if there are no boundaries. This assumption does not affect the coverage performance of users located at the cell center. However, this

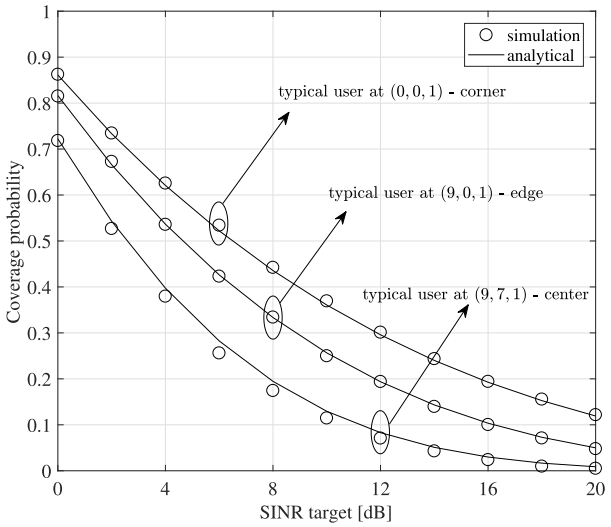

Fig. 12. Coverage probability of a typical user at different locations. $\tilde{\lambda}_{\mathrm{a}} = 0.1$ and $L = 2$ m.

assumption is not valid for users located at the room boundaries, as they generally receive less interference. We show in Fig. 12 that after certain adjustments, the derived analytical expressions are also applicable to users at room boundaries. In particular, the coverage probability of a typical user located at the room edge can still be calculated from Theorem 3 after replacing $\tilde{\lambda}_{\mathrm{a}}$ with $\tilde{\lambda}_{\mathrm{a}}/2$. Similarly, the coverage probability of a typical user located at the room corner can be calculated by replacing $\tilde{\lambda}_{\mathrm{a}}$ with $\tilde{\lambda}_{\mathrm{a}}/4$. It can be seen from Fig. 12 that after adjustment the proposed analytical framework is still accurate.

VI. Conclusions

In this paper, we provide a new analytical framework for the coverage analysis of multiuser VLC networks, taking into account the idle probability of APs that is evident especially in underloaded networks as well as general networks that operate with an AP sleep strategy to save energy and/or minimize the co-channel interference. By using mathematical tools from stochastic geometry and statistical-equivalent transformation, analytical expressions for the coverage probability are derived and given in tractable forms. Based on the derived results, it is shown that not only the density of APs, but also the density of users, has a significant impact on the coverage performance. The homogeneous PPP assumption for active APs is shown to be valid in general and gives close coverage results to the exact ones when the density of users is no smaller than the density of APs. We also show that, for typical receiver noise levels (~ -117.0 dBm), the SINR can be well approximated by the SIR for simplified coverage performance analysis in multiuser VLC networks.

A detailed evaluation of the applicability of the PPP model to VLC networks can be our future work. Further extensions of this work could include more realistic channel and blockage models. It is also of interest to generalize the proposed analytical framework to incorporate cell coordinations.

Appendix

A. Proof of Theorem 1

The Laplace transform of the ISR is formulated as:

$$\begin{aligned}\mathcal{L}_{\mathsf{ISR}}(s) &= \mathbb{E}\left[\exp(-s\mathsf{ISR})\right] \\ &= \mathbb{E}\left[\prod_{x_i\in\tilde{\Phi}_{\mathrm{a}}\setminus\{x_0\}} \exp\left(-s\left(\frac{x_i^2+L^2}{x_0^2+L^2}\right)^{-(m+3)}\right)\right] \\ &= \mathbb{E}_{x_0}\left[\mathbb{E}_{\tilde{\Phi}_{\mathrm{a}}}\left[\prod_{x_i\in\tilde{\Phi}_{\mathrm{a}}\setminus\{x_0\}} \omega(x_i)\,\middle|\, x_0\right]\right], \qquad (29)\end{aligned}$$

in which function $\omega(x_i)$ is defined as $\omega(x_i) = \exp\left(-s\left((x_i^2+L^2)/(x_0^2+L^2)\right)^{-(m+3)}\right)$. With the use of the probability generating functional (PGFL) of the PPP [15], the inner expectation of (29) can be calculated as:

$$\begin{aligned}&\mathbb{E}_{\tilde{\Phi}_{\mathrm{a}}}\left[\prod_{x_i\in\tilde{\Phi}_{\mathrm{a}}\setminus\{x_0\}} \omega(x_i)\,\middle|\, x_0\right] \\ &= \exp\left(-2\pi\tilde{\lambda}_{\mathrm{a}}\int_{x_0}^{\infty} x\left(1-\omega(x)\right)\mathrm{d}x\right) \\ &= \exp\left(-\pi\tilde{\lambda}_{\mathrm{a}}\int_1^{\infty}(x_0^2+L^2)\left(1-\exp\left(-sz^{-(m+3)}\right)\right)\mathrm{d}z\right), \qquad (30)\end{aligned}$$

where the last step follows from the change of variable $z = (x^2+L^2)/(x_0^2+L^2)$. Plugging (30) into (29) yields:

$$\begin{aligned}\mathcal{L}_{\mathsf{ISR}}(s) &= 2\pi\tilde{\lambda}_{\mathrm{a}}\int_0^{\infty} x_0 \exp\Bigg[-\pi\tilde{\lambda}_{\mathrm{a}}x_0^2 - \pi\tilde{\lambda}_{\mathrm{a}}\int_1^{\infty}(x_0^2+L^2) \\ &\qquad\times\left(1-\exp\left(-sz^{-(m+3)}\right)\right)\mathrm{d}z\Bigg]\mathrm{d}x_0 \\ &= 2\pi\tilde{\lambda}_{\mathrm{a}}\int_0^{\infty} x_0\exp\left(-\pi\tilde{\lambda}_{\mathrm{a}}x_0^2(1+W(s))\right)\mathrm{d}x_0 \\ &\qquad\times\exp\left(-\pi\tilde{\lambda}_{\mathrm{a}}L^2W(s)\right), \qquad (31)\end{aligned}$$

where function $W(s)$ is defined as:

$$\begin{aligned}W(s) &= \int_1^{\infty}\left(1-\exp\left(-sz^{-(m+3)}\right)\right)\mathrm{d}z \\ &= z\left(1-\frac{1}{m+3}E_{\frac{m+4}{m+3}}\left(sz^{-(m+3)}\right)\right)\Bigg|_{z=1}^{\infty} \\ &= -1+\frac{1}{m+3}E_{\frac{m+4}{m+3}}(s)+\Gamma\left(\frac{m+2}{m+3}\right)s^{\frac{1}{m+3}}. \qquad (32)\end{aligned}$$

Furthermore, the integration (31) can be simplified to:

$$\begin{aligned}&2\pi\tilde{\lambda}_{\mathrm{a}}\int_0^{\infty} x_0\exp\left(-\pi\tilde{\lambda}_{\mathrm{a}}x_0^2(1+W(s))\right)\mathrm{d}x_0 \\ &= -\frac{1}{1+W(s)}\exp\left(-\pi\tilde{\lambda}_{\mathrm{a}}x_0^2(1+W(s))\right)\Bigg|_{x_0=0}^{\infty} \\ &= \frac{1}{1+W(s)}. \qquad (33)\end{aligned}$$

Combining (31) – (33), (13) is obtained.

B. Proof of Theorem 2

Observe from (18) that the SINR model of interest is a function of the distance between the typical user and APs only, but not a function of the azimuth. Therefore, the two-dimensional homogeneous PPP $\tilde{\Phi}_{\mathrm{a}}$, which models the horizontal distance between the typical user and the AP, is statistically equivalent to another one-dimensional inhomogeneous Poisson process $\tilde{\Phi}_{\mathrm{eq1}} = \{x_i, i \in \mathbb{N}\} \subset \mathbb{R}^1$, with density function $\tilde{\lambda}_{\mathrm{eq1}}(x) = \int_0^{2\pi} \tilde{\lambda}_{\mathrm{a}} x \mathrm{d}\theta = 2\pi\tilde{\lambda}_{\mathrm{a}} x$. The SINR model for $\tilde{\Phi}_{\mathrm{eq1}}$ is the same as the one for $\tilde{\Phi}_{\mathrm{a}}$, i.e., $\mathsf{SINR}_{\mathrm{eq1}} = \mathsf{SINR}$. Define a path loss function $\ell(x) = (x^2 + L^2)^{m+3}$, whose inverse can be calculated as $\ell^{-1}(x) = \left(x^{1/(m+3)} - L^2\right)^{1/2}$. Since the path-loss function ℓ has a continuous inverse, this newly mapped process $\tilde{\Phi}_{\mathrm{eq2}} = \{\ell_i, i \in \mathbb{N}\} \subset \mathbb{R}^1$ is also a PPP, generally an inhomogeneous one, according to the mapping theorem [17]. The density function of $\tilde{\Phi}_{\mathrm{eq2}}$, denoted by $\tilde{\lambda}_{\mathrm{eq2}}(\ell)$, can be calculated from the statistical equivalence:

$$\mathbb{E}_{\tilde{\Phi}_{\mathrm{eq2}}}\left[\sum_{\ell_i \in \tilde{\Phi}_{\mathrm{eq2}}} \mathbf{1}_{[\underline{\ell},\bar{\ell}]}(\ell_i)\right] = \mathbb{E}_{\tilde{\Phi}_{\mathrm{eq1}}}\left[\sum_{x_i \in \tilde{\Phi}_{\mathrm{eq1}}} \mathbf{1}_{[\underline{x},\bar{x}]}(x_i)\right], \quad (34)$$

where $[\underline{\ell}, \bar{\ell}]$, with $L^{2(m+3)} \leq \underline{\ell} \leq \bar{\ell}$, is an arbitrary but nonempty interval forming a subset of $\tilde{\Phi}_{\mathrm{eq2}}$, $\underline{x} = \left(\underline{\ell}^{1/(m+3)} - L^2\right)^{1/2}$ and $\bar{x} = \left(\bar{\ell}^{1/(m+3)} - L^2\right)^{1/2}$. Rewriting (34) in terms of the density function for both processes yields:

$$\begin{aligned}\int_{\underline{\ell}}^{\bar{\ell}} \tilde{\lambda}_{\mathrm{eq2}}(\ell)\mathrm{d}\ell &= \int_{\underline{x}}^{\bar{x}} \tilde{\lambda}_{\mathrm{eq1}}(x)\mathrm{d}x \\ &= \int_{\underline{\ell}}^{\bar{\ell}} \tilde{\lambda}_{\mathrm{eq1}}\left(\sqrt{\ell^{\frac{1}{m+3}} - L^2}\right) \frac{1}{m+3} \frac{\ell^{\frac{1}{m+3}-1}}{2\sqrt{\ell^{\frac{1}{m+3}} - L^2}}\mathrm{d}\ell. \quad (35)\end{aligned}$$

From (35), $\tilde{\lambda}_{\mathrm{eq2}}(\ell)$ can be obtained as:

$$\tilde{\lambda}_{\mathrm{eq2}}(\ell) = \frac{\pi\tilde{\lambda}_{\mathrm{a}}}{m+3}\ell^{\frac{1}{m+3}-1}, \quad (36)$$

for $\ell > L^{2(m+3)}$ and zero otherwise. Since the density of $\tilde{\Phi}_{\mathrm{eq2}}$ is found to be a varying function of the distance, it is indeed an inhomogeneous process. Because of the mapping from x to ℓ, the SINR model for $\tilde{\Phi}_{\mathrm{eq2}}$ should be changed accordingly to:

$$\mathsf{SINR}_{\mathrm{eq2}} = \frac{\ell_0^{-1}}{\sum\limits_{\ell_i \in \tilde{\Phi}_{\mathrm{eq2}}\setminus\{\ell_0\}} \ell_i^{-1} + \bar{\sigma}^2}. \quad (37)$$

By letting $\ell^{-1} = gx^{-1}$, we arrive at the SINR model shown in (20). Again, using the mapping theorem [17], we have the following result based on the statistical equivalence property between $\tilde{\Phi}_{\mathrm{eq2}}$ and $\tilde{\Phi}_{\mathrm{eq}}$:

$$\mathbb{E}_{\tilde{\Phi}_{\mathrm{eq2}}}\left[\sum_{\ell_i \in \tilde{\Phi}_{\mathrm{eq2}}} \mathbf{1}_{[\underline{\ell},\bar{\ell}]}(\ell_i)\right] = \mathbb{E}_{g,\tilde{\Phi}_{\mathrm{eq}}}\left[\sum_{x_i \in \tilde{\Phi}_{\mathrm{eq}}} \mathbf{1}_{[\underline{x},\bar{x}]}(x_i)\right], \quad (38)$$

where $\underline{x} = g\underline{\ell}$ and $\bar{x} = g\bar{\ell}$. Furthermore, (38) can be rewritten in the integral form:

$$\begin{aligned}\int_{\underline{\ell}}^{\bar{\ell}} \tilde{\lambda}_{\mathrm{eq2}}(\ell)\mathrm{d}\ell &= \mathbb{E}_g\left[\int_{\underline{x}}^{\bar{x}} \tilde{\lambda}_{\mathrm{eq}}(x)\mathrm{d}x\right] \\ &= \int_{\underline{\ell}}^{\bar{\ell}} \mathbb{E}_g\left[g\tilde{\lambda}_{\mathrm{eq}}(g\ell)\right]\mathrm{d}\ell \\ &= \int_{\underline{\ell}}^{\bar{\ell}} \int_0^{\infty} g\tilde{\lambda}_{\mathrm{eq}}(g\ell)\exp(-g)\mathrm{d}g\mathrm{d}\ell. \quad (39)\end{aligned}$$

After plugging (36) into (39) and using integral equality $\int_0^{\infty} g^{\frac{1}{m+3}}\exp(-g)\mathrm{d}g = \Gamma\left(\frac{m+4}{m+3}\right)$, we have:

$$\begin{aligned}&\int_0^{\infty} g\tilde{\lambda}_{\mathrm{eq}}(g\ell)\exp(-g)\mathrm{d}g \\ &\quad= \int_0^{\infty} \frac{\pi\tilde{\lambda}_{\mathrm{a}}}{m+3}\frac{1}{\Gamma\left(\frac{m+4}{m+3}\right)}\ell^{\frac{1}{m+3}-1} g^{\frac{1}{m+3}}\exp(-g)\mathrm{d}g. \quad (40)\end{aligned}$$

With some simplifications, $\tilde{\lambda}_{\mathrm{eq}}(g\ell)$ can be obtained as:

$$\tilde{\lambda}_{\mathrm{eq}}(g\ell) = \frac{\pi\tilde{\lambda}_{\mathrm{a}}}{m+3}\frac{1}{\Gamma\left(\frac{m+4}{m+3}\right)}(g\ell)^{\frac{1}{m+3}-1}, \quad (41)$$

which is equivalent to (19). To this end, Theorem 2 is proved.

C. Proof of Theorem 3

Based on the statistical equivalence between $\tilde{\Phi}_{\mathrm{a}}$ and $\tilde{\Phi}_{\mathrm{eq}}$, the coverage probability can alternatively be calculated as:

$$\begin{aligned}&\mathbb{P}\left[\mathsf{SINR} > T\right] \\ &= \mathbb{P}\left[\mathsf{SINR}_{\mathrm{eq}} > T\right] \\ &= \mathbb{P}\left[\frac{g_0\, x_0^{-1}}{\sum\limits_{x_i \in \tilde{\Phi}_{\mathrm{eq}}\setminus\{x_0\}} g_i x_i^{-1} + \bar{\sigma}^2} > T\right] \\ &= \mathbb{E}_{g,\tilde{\Phi}_{\mathrm{eq}}}\left[\mathbb{P}\left[g_0 > T x_0\left(\sum_{x_i \in \tilde{\Phi}_{\mathrm{eq}}\setminus\{x_0\}} g_i x_i^{-1} + \bar{\sigma}^2\right)\middle| x_0\right]\right] \\ &= \mathbb{E}_{g,\tilde{\Phi}_{\mathrm{eq}}}\left[\exp\left(-T\bar{\sigma}^2 x_0\right)\prod_{x_i \in \tilde{\Phi}_{\mathrm{eq}}\setminus\{x_0\}} \exp\left(-T g_i x_i^{-1} x_0\right)\right], \quad (42)\end{aligned}$$

where the last step is obtained from the exponential distribution characteristic of the introduced auxiliary variable g_0. Based on Slivnyak's theorem [15], the calculation of (42) can be simplified by first conditioning on x_0 and then averaging the result with respect to x_0, since conditioning on x_0 does not change the distribution of $x_i \in \tilde{\Phi}_{\mathrm{eq}}\setminus\{x_0\}$. Also, due to the i.i.d. property of g_i and its further independence from $\tilde{\Phi}_{\mathrm{eq}}$, the coverage probability of the typical user can be calculated

with the use of PGFL of the PPP:

$$\mathbb{P}\left[\mathsf{SINR} > T\right] = \mathbb{E}_{x_0}\Bigg[\exp\left(-T\bar{\sigma}^2\, x_0\right)\exp\Bigg[-\int_{L^{2(m+3)}}^{\infty}\tilde{\lambda}_{\mathrm{eq}}(x) \times \left(1-\mathbb{E}_g\left[\exp\left(-Tgx^{-1}x_0\right)\right]\right)\mathrm{d}x\Bigg]\Bigg], \tag{43}$$

in which the inner expectation with respect to the auxiliary variable is found to be:

$$\mathbb{E}_g\left[\exp\left(-Tgx^{-1}x_0\right)\right] = \int_0^{\infty}\exp\left(-Tgx^{-1}x_0\right)\exp(-g)\mathrm{d}g = \frac{1}{1+Tx^{-1}x_0}. \tag{44}$$

Plugging (19) and (44) into (43) yields:

$$\mathbb{P}\left[\mathsf{SINR}>T\right] = \mathbb{E}_{x_0}\left[\exp\left(-T\bar{\sigma}^2x_0\right)\exp\left[-\frac{\pi\tilde{\lambda}_{\mathrm{a}}}{\Gamma\left(\frac{1}{m+3}\right)} \times \int_{L^{2(m+3)}}^{\infty}x^{\frac{1}{m+3}-1}\left(1-\frac{1}{1+Tx^{-1}x_0}\right)\mathrm{d}x\right]\right], \tag{45}$$

in which the inner integration can be calculated as:

$$\int_{L^{2(m+3)}}^{\infty}x^{\frac{1}{m+3}-1}\left(1-\frac{1}{1+Tx^{-1}x_0}\right)\mathrm{d}x = \frac{m+3}{m+2}L^{-2(m+2)}Tx_0{}_2F_1\left(1,\frac{m+2}{m+3};\frac{2m+5}{m+3};-L^{-2(m+3)}Tx_0\right). \tag{46}$$

With a slight abuse of notation, we denote by SINR_i the SINR achieved at the typical user when it receives information signal from AP i and interference from all other APs. It has been shown in (5) that the typical user is associated with the nearest AP in its vicinity. Therefore, we have $\mathsf{SINR} = \mathsf{SINR}_0$. Since $x_0 \le x_1 \le \cdots$ holds by definition, it is straightforward that for $i = 1, 2, \cdots$, $\mathsf{SINR}_i = (x_i^2+L^2)^{-(m+3)} \Big/ \left(\sum_{x_j\in\tilde{\Phi}_{\mathrm{a}}\setminus\{x_i\}}(x_j^2+L^2)^{-(m+3)}+\bar{\sigma}^2\right) < 1$. This is equivalent to $\mathbb{P}[\mathsf{SINR}_i > 1] = 0$. As a result, when $T > 1$, the coverage probability can now be expressed as $\mathbb{P}[\mathsf{SINR} > T] = \mathbb{P}[\mathsf{SINR}_0 > T] = \sum_{i=0}^{\infty}\mathbb{P}[\mathsf{SINR}_i > T]$, which gives:

$$\mathbb{P}\left[\mathsf{SINR} > T\right] = \mathbb{E}_{\tilde{\Phi}_{\mathrm{eq}}}\left[\sum_{x\in\tilde{\Phi}_{\mathrm{eq}}}\exp\left(-T\bar{\sigma}^2x\right)\exp\left[-\frac{\pi\tilde{\lambda}_{\mathrm{a}}}{m+2}\frac{L^{-2(m+2)}}{\Gamma\left(\frac{m+4}{m+3}\right)}Tx \times {}_2F_1\left(1,\frac{m+2}{m+3};\frac{2m+5}{m+3};-L^{-2(m+3)}Tx\right)\right]\right]. \tag{47}$$

After applying Campbell's Theorem [15] and inserting (19) into (47), (21) is obtained.

D. Numerical Computation of the Coverage Probability in (21)

Using the Gauss-Chebyshev Quadrature (GCQ) rule [31], the integration in (21) can be numerically calculated as a finite sum with N_{GCQ} terms:

$$\mathbb{P}\left[\mathsf{SINR}>T\right] \approx \sum_{u=1}^{N_{\mathrm{GCQ}}}w_{(u)}\frac{\pi\tilde{\lambda}_{\mathrm{a}}}{\Gamma\left(\frac{1}{m+3}\right)}x_{(u)}^{\frac{1}{m+3}-1}\exp\left(-T\bar{\sigma}^2x_{(u)}\right) \times \exp\left[-\frac{\pi\tilde{\lambda}_{\mathrm{a}}}{m+2}\frac{L^{-2(m+2)}}{\Gamma\left(\frac{m+4}{m+3}\right)}Tx_{(u)}S_{N_{\mathrm{tol}}}(x_{(u)})\right], \tag{48}$$

where $w_{(u)}$ and $x_{(u)}$, for $u = 1, 2, \cdots, N_{\mathrm{GCQ}}$, are weights and abscissas of the quadrature, respectively [31]. $S_{N_{\mathrm{tol}}}(x_{(u)})$ is the numerical value of the Gauss hypergeometric function evaluated at $x = x_{(u)}$, and it can be computed as follows. From basic Taylor series expansion, the Gauss hypergeometric function at $x_{(u)}$ can be written as [32]:

$$ {}_2F_1\left(1,\frac{m+2}{m+3};\frac{2m+5}{m+3};-L^{-2(m+3)}Tx_{(u)}\right) = \sum_{q=0}^{\infty}\frac{(1)_q\left(\frac{m+2}{m+3}\right)_q}{\left(\frac{2m+5}{m+3}\right)_q}\frac{1}{q!}\left(-L^{-2(m+3)}Tx_{(u)}\right)^q, \tag{49}$$

where $(z)_q$ is the rising Pochhammer symbol, defined as:

$$(z)_q = \begin{cases}1, & q=0,\\ z(z+1)\cdots(z+q-1), & q=1,2,\cdots,.\end{cases} \tag{50}$$

The summation of the first q terms of (49), denoted by $S_q(x_{(u)})$, can be computed through following steps:

$$\begin{aligned}
&S_0(x_{(u)}) = 1,\\
&S_1(x_{(u)}) = \frac{m+2}{2m+5}\left(-L^{-2(m+3)}Tx_{(u)}\right),\\
&\quad q = 2,\\
&\textbf{Do}\quad b_q = \frac{q(m+3)-1}{(q+1)(m+3)-1},\\
&\quad S_q(x_{(u)}) = S_{q-1}(x_{(u)}) + (S_{q-1}(x_{(u)}) - S_{q-2}(x_{(u)})) \times b_q\left(-L^{-2(m+3)}Tx_{(u)}\right),\\
&\quad q = q+1,\\
&\textbf{Until}\ \frac{|S_{N_{\mathrm{tol}}+1}(x_{(u)}) - S_{N_{\mathrm{tol}}}(x_{(u)})|}{|S_{N_{\mathrm{tol}}}(x_{(u)})|} \le \mathrm{tol}\ \&\\
&\quad \frac{|S_{N_{\mathrm{tol}}}(x_{(u)}) - S_{N_{\mathrm{tol}}-1}(x_{(u)})|}{|S_{N_{\mathrm{tol}}-1}(x_{(u)})|} \le \mathrm{tol}\ \&\\
&\quad \frac{|S_{N_{\mathrm{tol}}-1}(x_{(u)}) - S_{N_{\mathrm{tol}}-2}(x_{(u)})|}{|S_{N_{\mathrm{tol}}-2}(x_{(u)})|} \le \mathrm{tol},
\end{aligned}$$

where tol is some tolerance, and $S_{N_{\mathrm{tol}}}(x_{(u)})$ is the returned numerical solution for ${}_2F_1\left(1,\frac{m+2}{m+3};\frac{2m+5}{m+3};-L^{-2(m+3)}Tx_{(u)}\right)$. Note that the maximum number of iterations required for calculating (49) is not fixed. For typical values of T ($0 \le T \le 100$), 200 recursions of q are found to be sufficient for the computation of the coverage probability.

REFERENCES

[1] T. Komine and M. Nakagawa, "Fundamental analysis for visible-light communication system using LED lights," *IEEE Trans. Consum. Electron.*, vol. 50, no. 1, pp. 100–107, Feb. 2004.

[2] J. Grubor, S. Randel, K. D. Langer, and J. W. Walewski, "Broadband information broadcasting using LED-based interior lighting," *J. Lightw. Technol.*, vol. 26, no. 24, pp. 3883–3892, Dec. 15, 2008.

[3] H. Haas, L. Yin, Y. Wang, and C. Chen, "What is LiFi?" *J. Lightw. Technol.*, vol. 34, no. 6, pp. 1533–1544, Mar. 15, 2016.

[4] *IEEE Standard for Local and Metropolitan Area Networks—Part 15.7: Short-Range Wireless Optical Communication Using Visible Light*, IEEE Standard 802.15.7-2011, 2011.

[5] H. Haas, "High-speed wireless networking using visible light," *SPIE Newsroom*, vol. 1, pp. 1–3, Apr. 2013.

[6] L. Zeng *et al.*, "High data rate multiple input multiple output (MIMO) optical wireless communications using white LED lighting," *IEEE J. Sel. Areas Commun.*, vol. 27, no. 9, pp. 1654–1662, Dec. 2009.

[7] B. Li, J. Wang, R. Zhang, H. Shen, C. Zhao, and L. Hanzo, "Multiuser MISO transceiver design for indoor downlink visible light communication under per-LED optical power constraints," *IEEE Photon. J.*, vol. 4, no. 7, Aug. 2015, Art. no. 7201415.

[8] K. Ying, H. Qian, R. J. Baxley, and S. Yao, "Joint optimization of precoder and equalizer in MIMO VLC systems," *IEEE J. Sel. Areas Commun.*, vol. 33, no. 9, pp. 1949–1958, Sep. 2015.

[9] H. Ma, L. Lampe, and S. Hranilovic, "Coordinated broadcasting for multiuser indoor visible light communication systems," *IEEE Trans. Commun.*, vol. 63, no. 9, pp. 3313–3324, Sep. 2015.

[10] M. Kashef, M. Abdallah, K. Qaraqe, H. Haas, and M. Uysal, "Coordinated interference management for visible light communication systems," *J. Opt. Commun. Netw.*, vol. 7, no. 11, pp. 1098–1108, Nov. 2015.

[11] R. Zhang, J. Wang, Z. Wang, Z. Xu, C. Zhao, and L. Hanzo, "Visible light communications in heterogeneous networks: Paving the way for user-centric design," *IEEE Wireless Commun.*, vol. 22, no. 2, pp. 8–16, Apr. 2015.

[12] J. Lian and M. Brandt-Pearce, "Distributed power allocation for multi-user MISO indoor visible light communications," in *Proc. IEEE Global Commun. Conf. (GLOBECOM)*, San Diego, CA, USA, Dec. 2015, pp. 1–7.

[13] D. Bykhovsky and S. Arnon, "Multiple access resource allocation in visible light communication systems," *J. Lightw. Technol.*, vol. 32, no. 8, pp. 1594–1600, Apr. 15, 2014.

[14] C. Chen, D. A. Basnayaka, and H. Haas, "Downlink performance of optical attocell networks," *J. Lightw. Technol.*, vol. 34, no. 1, pp. 137–156, Jan. 1, 2016.

[15] S. N. Chiu, D. Stoyan, W. S. Kendall, and J. Mecke, *Stochastic Geometry and Its Applications*, 2nd ed. Hoboken, NJ, USA: Wiley, 1996.

[16] J. G. Andrews, F. Baccelli, and R. K. Ganti, "A tractable approach to coverage and rate in cellular networks," *IEEE Trans. Commun.*, vol. 59, no. 11, pp. 3122–3134, Nov. 2011.

[17] A. Baddeley, I. Bárány, R. Schneider, and W. Weil, *Stochastic Geometry* (Lecture Notes in Mathematics). Berlin, Germany: Springer-Verlag, 2007.

[18] H. ElSawy, A. Sultan-Salem, M.-S. Alouini, and M. Z. Win, "Modeling and analysis of cellular networks using stochastic geometry: A tutorial," *IEEE Commun. Surveys Tuts.*, vol. 19, no. 1, pp. 167–203, 1st Quart., 2017.

[19] J. M. Kahn and J. R. Barry, "Wireless infrared communications," *Proc. IEEE*, vol. 85, no. 2, pp. 265–298, Feb. 1997.

[20] L. Yin, W. O. Popoola, X. Wu, and H. Haas, "Performance evaluation of non-orthogonal multiple access in visible light communication," *IEEE Trans. Commun.*, vol. 64, no. 12, pp. 5162–5175, Dec. 2016.

[21] S. Dimitrov, S. Sinanovic, and H. Haas, "Clipping noise in OFDM-based optical wireless communication systems," *IEEE Trans. Commun.*, vol. 60, no. 4, pp. 1072–1081, Apr. 2012.

[22] J.-S. Ferenc and Z. Néda, "On the size distribution of Poisson Voronoi cells," *Phys. A, Stat. Mech. Appl.*, vol. 385, no. 2, pp. 518–526, Nov. 2007.

[23] S. Lee and K. Huang, "Coverage and economy of cellular networks with many base stations," *IEEE Commun. Lett.*, vol. 16, no. 7, pp. 1038–1040, Jul. 2012.

[24] C. Li, J. Zhang, and K. B. Letaief, "Throughput and energy efficiency analysis of small cell networks with multi-antenna base stations," *IEEE Trans. Wireless Commun.*, vol. 13, no. 5, pp. 2505–2517, May 2014.

[25] I. S. Gradshteyn and I. M. Ryzhik, *Table of Integrals, Series, and Products*, 7th ed. San Diego, CA, USA: Academic, 2007.

[26] K. Nakagawa, "Application of Tauberian theorem to the exponential decay of the tail probability of a random variable," *IEEE Trans. Inf. Theory*, vol. 53, no. 9, pp. 3239–3249, Sep. 2007.

[27] P. Madhusudhanan, J. G. Restrepo, Y. Liu, T. X. Brown, and K. R. Baker, "Downlink performance analysis for a generalized shotgun cellular system," *IEEE Trans. Wireless Commun.*, vol. 13, no. 12, pp. 6684–6696, Dec. 2014.

[28] H. R. Thompson, "Distribution of distance to Nth neighbour in a population of randomly distributed individuals," *Ecology*, vol. 37, no. 2, pp. 391–394, Apr. 1956.

[29] A. M. Khalid, G. Cossu, R. Corsini, P. Choudhury, and E. Ciaramella, "1-Gb/s transmission over a phosphorescent white LED by using rate-adaptive discrete multitone modulation," *IEEE Photon. J.*, vol. 4, no. 5, pp. 1465–1473, Oct. 2012.

[30] D. Tsonev *et al.*, "Brien, "A 3-Gb/s single-LED OFDM-based wireless VLC link using a gallium nitride μLED," *IEEE Photon. Technol. Lett.*, vol. 26, no. 7, pp. 637–640, Apr. 1, 2014.

[31] M. D. Renzo, "Stochastic geometry modeling and analysis of multi-tier millimeter wave cellular networks," *IEEE Trans. Wireless Commun.*, vol. 14, no. 9, pp. 5038–5057, Sep. 2015.

[32] Y. L. Luke, *The Special Functions and Their Approximations*. New York, NY, USA: Academic, 1969.

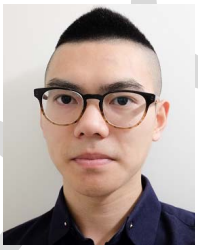

Liang Yin received the B.Eng. degree (Hons.) in electronics and electrical engineering from The University of Edinburgh, Edinburgh, U.K., in 2014, where he is currently pursuing the Ph.D. degree in electrical engineering. His research interests are in visible light communication and positioning, multi-user networking, and wireless network performance analysis. He was a recipient of the Class Medal Award and the IET Prize Award from The University of Edinburgh.

Harald Haas (S'98–AM'00–M'03–SM'17) received the Ph.D. degree from The University of Edinburgh in 2001. He currently holds the Chair of Mobile Communications at The University of Edinburgh, and is the Initiator, Co-Founder, and the Chief Scientific Officer of pureLiFi Ltd., and the Director of the LiFi Research and Development Center, The University of Edinburgh. He has authored 400 conference and journal papers, including a paper in *Science* and co-authored the book *Principles of LED Light Communications Towards Networked Li-Fi* (Cambridge University Press, 2015). His main research interests are in optical wireless communications, hybrid optical wireless and RF communications, spatial modulation, and interference coordination in wireless networks. He first introduced and coined spatial modulation and LiFi. LiFi was listed among the 50 best inventions in *TIME* Magazine 2011. He was an invited speaker at TED Global 2011, and his talk on "Wireless Data from Every Light Bulb" has been watched online over 2.4 million times. He gave a second TED Global lecture in 2015 on the use of solar cells as LiFi data detectors and energy harvesters. This has been viewed online over 1.8 million times. He was elected as a fellow of the Royal Society of Edinburgh in 2017. In 2012 and 2017, he was a recipient of the prestigious Established Career Fellowship from the Engineering and Physical Sciences Research Council (EPSRC) within Information and Communications Technology in the U.K. In 2014, he was selected by EPSRC as one of ten Recognising Inspirational Scientists and Engineers (RISE) Leaders in the U.K. He was a co-recipient of the EURASIP Best Paper Award for the *Journal on Wireless Communications and Networking* in 2015, and co-recipient of the Jack Neubauer Memorial Award of the IEEE Vehicular Technology Society. In 2016, he received the Outstanding Achievement Award from the International Solid State Lighting Alliance. He was a co-recipient of recent best paper awards at VTC-Fall, 2013, VTC-Spring 2015, ICC 2016, and ICC 2017. He is an Editor of the IEEE TRANSACTIONS ON COMMUNICATIONS and the IEEE JOURNAL OF LIGHTWAVE TECHNOLOGIES.

Coverage Analysis of Multiuser Visible Light Communication Networks

Liang Yin and Harald Haas, *Senior Member, IEEE*

***Abstract*— In this paper, a new mathematical framework for the coverage probability analysis of multiuser visible light communication (VLC) networks is presented. It takes into account the idle probability of access points (APs) that are not associated with any users and hence do not function as the source of interference. The idle probability of APs is evident especially in underloaded networks as well as general networks that operate with an AP sleep strategy to save energy and/or minimize the co-channel interference. Due to the absence of the "multipath fading" effect, the evaluation of the distribution function of the signal-to-interference-plus-noise ratio (SINR) is more challenging in VLC networks than in radio frequency-based cellular networks. By using the statistical-equivalent transformation of the SINR, analytical expressions for the coverage probability are derived and given in tractable forms. Comparing the derived results with extensive Monte Carlo simulations, we show that assuming a thinned homogeneous Poisson point process for modeling active APs is valid in general, and it gives close results to the exact ones when the density of users is no less than the density of APs in the network. Both analytical and simulation results show that, for typical receiver noise levels (~ -117 dBm), approximating the SINR by the signal-to-interference ratio is sufficiently accurate for the coverage analysis in VLC networks.**

***Index Terms*— Visible light communication, light-emitting diode, coverage probability, Poisson point process, stochastic geometry.**

I. Introduction

CURRENT wireless networks are experiencing difficulties in keeping pace with the exponential growth of wireless devices that require higher data rate and seamless service coverage. Such imminent problems have motivated many industry partners and research communities to seek new technologies for wireless communication. Among many candidate solutions, visible light communication (VLC) [1]–[3] has been acknowledged as a promising technology to address the scarcity of radio frequency (RF) spectra, due to its advantages in modulation bandwidth, data rate, frequency reuse factor and link security. Extensive studies on point-to-point VLC transmission and reception techniques during the past decade have also led to the recent standardization of VLC for short-range applications: IEEE 802.15.7 [4]. A revision to the current standard is also in progress.

Small-cell deployment for heterogeneous cellular networks has proven to be effective in improving the network throughput and spectral efficiency. The femtocell-like deployment of VLC in indoor environments leads to the concept of optical attocells [5], where each light-emitting diode (LED) acts as an optical access point (AP) to serve multiple users within its coverage. Since then, many research efforts have been given to the design and analysis of multiuser VLC networks. Topics include multiple-input multiple-output (MIMO) transmission [6], transceiver design [7], precoder and equalizer design [8], AP coordination [9], interference mitigation [10], user scheduling [11] and resource allocation and optimization [12], [13], to name just a few.

A. Related Work and Motivation

System-level performance of multiuser VLC networks is typically evaluated with the aid of computer simulations. They are often complicated, time-consuming and unable to provide many insights into how the performance is affected by various parameters in the network. The analytical evaluation, on the other hand, is generally not straightforward due to the lack of accurate and at the same time analytically tractable models. The most common approach for modeling the location of optical APs is based on the grid model, where LED lights are installed in the ceiling with a regular pattern [1], [2], [6], [9], [13], [14]. The evaluation of the grid based network is recognized to be analytically difficult and hence is normally done with computer simulation, which has also motivated the authors in [14] to use stochastic models [15]–[18] for the performance evaluation. Compared to the grid model, stochastic models are more mathematically tractable. More importantly, the following observations indicate that in some scenarios a stochastic model is required in order to accurately characterize the performance of VLC networks. Firstly, modern LED lights with built-in motion detection sensors are widely deployed in public spaces to reduce energy consumption. In this scenario, some of the LED lights are temporarily switched off when they are not required to provide illumination. Also, even when switched on, some of the LEDs can turn off their wireless communication functionality when no data traffic is demanded from them, for

Manuscript received May 3, 2017; revised September 27, 2017; accepted December 8, 2017. The work of H. Haas was supported by the U.K. Engineering and Physical Sciences Research Council under Grant EP/K008757/1. The associate editor coordinating the review of this paper and approving it for publication was M. Uysal. *(Corresponding author: Liang Yin.)*

The authors are with the Li-Fi Research and Development Centre, School of Engineering, Institute for Digital Communications, The University of Edinburgh, Edinburgh EH9 3JL, U.K. (e-mail: l.yin@ed.ac.uk; h.haas@ed.ac.uk).

Color versions of one or more of the figures in this paper are available online at http://ieeexplore.ieee.org.

Digital Object Identifier 10.1109/TWC.2017.2782694

example, relying on an AP sleep strategy. In these scenarios, the distribution of APs cannot be accurately modeled by the grid model. Instead, a stochastic thinning process built upon the grid-like deployment of LEDs is more accurate. However, modeling this stochastic thinning process requires full knowledge of the users' movement and handover characteristics, which is not analytically tractable. Secondly, the distribution of active APs in a VLC network is generally variable, and it changes dynamically due to the random movement of users. Thirdly, the grid model is not applicable in scenarios where not only ceiling lights but also LED screens, reading lamps, and other "smart" lights are an integral part of the network architecture, in which the deployment of VLC APs appears to be more stochastic. For these reasons and in order to obtain analytically tractable results, the PPP model is of our focus in this work.

To the best of authors' knowledge, [14] is the only published work that reports on the performance of multiuser VLC networks using the stochastic model. The distribution function of the signal-to-interference-plus-noise ratio (SINR) of a typical user in the network reported in [14] was given as a sum of Gamma densities, whose calculation requires Gram-Charlier series expansion with infinite terms and Laguerre polynomials. As a result, computing the distribution function of the SINR would involve complicated integrals and infinite sums. Motivated by this, we report in this paper a new and simpler method for the characterization of the density function of the SINR by exploring powerful mathematical tools from stochastic geometry [15]–[18]. Furthermore, the analysis in [14] overlooks the probability of empty cells, in which APs are idle and hence do not act as the source of interference. This is especially evident in underloaded networks as well as general networks that use an AP sleep strategy.

Stochastic geometry has been widely used in cellular networks for modeling the locations of base stations (BSs) as a point process, usually a Poisson point process (PPP) [16] due to its mathematical tractability. Recent advances and results on stochastic geometry modeling of heterogeneous cellular networks can be found in a recent survey [18] and the rich references therein. Due to many fundamental differences between RF communication and VLC [3], existing results obtained for RF-based cellular networks can not be directly applied to VLC networks. Among many significant differences between RF and VLC, a noticeable one is their channel characteristics. More specifically, because the wavelength of visible light is hundreds of nanometers and the detection area of a typical VLC receiver, for example, a photodiode (PD), is millions of square wavelengths. This spatial diversity essentially prevents the "multipath fading" effect in VLC, which in turn makes the calculation of the density function of the SINR more challenging. Furthermore, in cellular networks, the vertical distance of the communication link is generally much smaller than the horizontal distance. Therefore, a planar system model is typically used. However, the size of attocells in VLC networks is in the order of meters. As a result, a three-dimensional system model considering both horizontal and vertical distances of the communication link is required in VLC networks.

B. Contributions

The contributions of this paper are summarized as follows.

1) We consider a three-dimensional attocell model and introduce an analytical framework for the coverage probability analysis in multiuser VLC networks. Based on the user-centric cell association, the proposed framework takes into account the idle probability of APs that are not associated with any users. Specifically, the analytical results are derived as a function of the user density, which is implicitly assumed to be infinity in the existing works [13], [14].
2) By assuming that the point process for the active APs in the network is a thinned homogeneous PPP, we derive an asymptotic result for the coverage probability in the low SINR regime. With the statistical-equivalent transformation, the exact coverage probability in the high SINR regime is derived and given in a mathematically tractable form. A simple and closed-form upper bound on the coverage probability is also provided. The coverage performance is evaluated in detail with various network parameters. We find that the homogeneous PPP assumption for modeling the location of active APs is generally valid, and it gives close results to the exact ones when the density of users is no less than the density of APs.
3) We investigate the effect of receiver noise on the network coverage performance. It is shown that, with typical receiver noise levels (~ -117.0 dBm), the SINR can be well approximated by the signal-to-interference ratio (SIR) for the performance analysis.

C. Paper Organization

The remainder of this paper is organized as follows. Section II describes the three-dimensional attocell model and formulates the SINR metric. With user-centric cell association, the idle probability of APs is derived in Section III. By assuming that the point process of active APs is a homogeneous PPP, analytical expressions for the coverage probability are derived in Section IV. In Section V, we provide numerical examples to validate the derived results and discuss the impact of various network parameters and assumptions on the coverage performance. Finally, Section VI gives the concluding remarks.

II. System Model

We consider a downlink transmission scenario in a multiuser VLC network, with full-frequency reuse, over a three-dimensional indoor space, as depicted in Fig. 1. The VLC APs are vertically fixed since they are attached to the room ceiling while their horizontal locations are modeled by a two-dimensional homogeneous PPP $\Phi_{\mathrm{a}} = \{x_i, i \in \mathbb{N}\} \subset \mathbb{R}^2$, with node density λ_{a}, where x_i is the horizontal distance between AP i and the origin.[1] Similarly, mobile users are also assumed to be at a fixed height, for example, at the desktop level, and

[1]We define the room center as the origin and use both notions interchangeably throughout the paper since the room center has more geographical meanings while the origin has more mathematical meanings in the theoretical analysis.

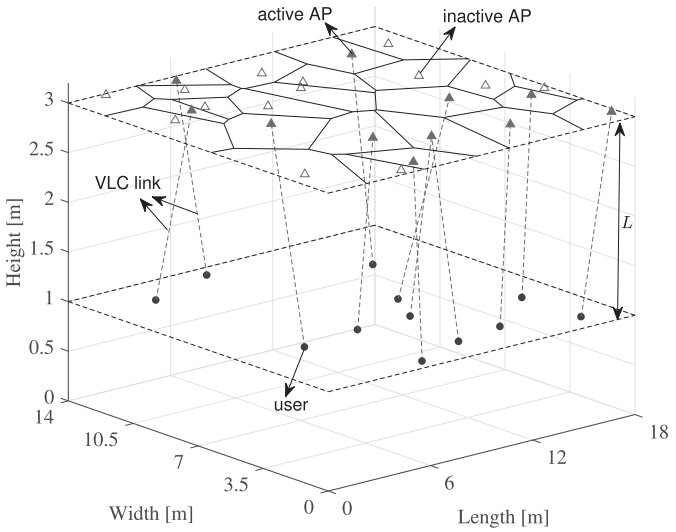

Fig. 1. Three-dimensional Voronoi cell formation in the VLC network assuming the nearest AP association: APs are randomly distributed in the ceiling following Φ_{a}, while users are randomly distributed at a lower horizontal plane following Φ_{u}. For the nearest AP association, each user is assumed to be served by the nearest AP in its vicinity.

their horizontal locations are modeled by another independent two-dimensional homogeneous PPP $\Phi_{\mathrm{u}} = \{y_j, j \in \mathbb{N}\} \subset \mathbb{R}^2$, with node density λ_{u}, where y_j is the horizontal distance between user j and the origin. The vertical separation between Φ_{a} and Φ_{u} is denoted by L. After adding an additional user at the room center, the new point process for mobile users becomes $\Phi_{\mathrm{u}} \cup \{0\}$. According to Slivnyak's theorem, adding a user into Φ_{u} is equivalent to conditioning Φ_{u} on the added point, and this does not change the distribution of original process Φ_{u} [15]. The homogeneity and motion-invariant property of the PPP [15] allow us to focus on a *typical* user located at an arbitrary location, and the obtained result would remain the same since it represents the average performance of all users in the network. This is true for an infinite network. For a finite network, the obtained result also remains unchanged, as long as the typical user is far away from room boundaries. This is justified by the power scaling law, stating that the received power is inversely proportional to the link distance and therefore quickly diminishes as the interfering AP is moved further away from the receiver. The origin is usually selected for the location of the typical user due to its notational simplicity. Therefore, in the following analysis, we focused on a typical user located at the origin and discuss the effect of room boundaries in detail in Section V. Note that in a practical VLC network, not all of the APs transmit signals at the same time. Hence, APs that are not in the "communication" mode can either be turned off or operate in the "illumination" mode only, and therefore they do not act as the source of interference in the network. As a result, from the communication perspective, the actual point process of active APs is no longer the same as Φ_{a} and can be determined by thinning PPP Φ_{a} to a new process $\tilde{\Phi}_{\mathrm{a}}$.

The complete VLC channel between an AP and a user includes both the line-of-sight (LOS) link and non-line-of-sight (NLOS) links, that are caused by light reflections of interior surfaces in the indoor environment. However, in a typical indoor environment, the signal power of NLOS components is significantly lower than that of the LOS link [1], [2], [6]. Therefore, we will only focus on the LOS link in the following analysis in order to obtain analytically tractable results and insights. Without loss of generality, the VLC AP is assumed to follow the Lambertian radiation profile, whose order can be calculated from $m = -1/\log_2(\cos(\Psi_{1/2}))$, where $\Psi_{1/2}$ denotes the semi-angle of the LED. The PD equipped at each user is assumed to be facing vertically upwards with a field-of-view (FOV) of Ψ_{fov}. For each VLC link, the direct current (DC) gain of the channel is given by [19]:

$$h = \frac{(m+1)A_{\mathrm{pd}}\eta}{2\pi d^2}\cos^m(\theta_{\mathrm{tx}})G_{\mathrm{f}}(\theta_{\mathrm{rx}})G_{\mathrm{c}}(\theta_{\mathrm{rx}})\cos(\theta_{\mathrm{rx}}), \quad (1)$$

where d is the Euclidean distance between the transmitter and receiver; A_{pd} denotes the effective detection area of the PD; η is the average responsivity of the PD in the white region; θ_{tx} and θ_{rx} are the angle of irradiance and the angle of incidence of the link, respectively; $G_{\mathrm{f}}(\theta_{\mathrm{rx}})$ represents the gain of the blue optical filter used at the receiver front end in order to obtain an improved modulation bandwidth; and $G_{\mathrm{c}}(\theta_{\mathrm{rx}})$ represents the gain of the optical concentrator, given by [19]:

$$G_{\mathrm{c}}(\theta_{\mathrm{rx}}) = \begin{cases} \dfrac{n_{\mathrm{c}}^2}{\sin^2(\Psi_{\mathrm{fov}})}, & 0 \le \theta_{\mathrm{rx}} \le \Psi_{\mathrm{fov}} \\ 0, & \theta_{\mathrm{rx}} > \Psi_{\mathrm{fov}}, \end{cases} \quad (2)$$

where n_{c} is the reflective index of the optical concentrator, and it is defined as the ratio of the speed of light in vacuum and the phase velocity of light in the optical material. For visible light, typical values for n_{c} vary between 1 and 2.

Based on the geometric property [20] of the VLC link, we can obtain $d_i = \sqrt{x_i^2 + L^2}$, $\cos(\theta_{\mathrm{tx},i}) = L/\sqrt{x_i^2 + L^2}$ and $\cos(\theta_{\mathrm{rx},i}) = L/\sqrt{x_i^2 + L^2}$. As a result, the VLC channel gain from AP i to the typical user can be simplified to:

$$h_i(x_i) = \alpha(x_i^2 + L^2)^{-\frac{m+3}{2}}, \quad (3)$$

where $\alpha = (m+1)A_{\mathrm{pd}}\eta G_{\mathrm{f}}(\theta_{\mathrm{rx},i})G_{\mathrm{c}}(\theta_{\mathrm{rx},i})L^{m+1}/2\pi$. Denote by x^* the serving AP that gives the highest channel gain to the typical user. We can write

$$x^* = \arg\max_{x_i \in \Phi_{\mathrm{a}}} h_i(x_i) = x_0, \quad (4)$$

where x_0 is the nearest AP in Φ_{a} to the origin. It can be seen from (4) that the highest channel gain association is equivalent to the nearest AP association, resulting in coverage areas that form the Voronoi tessellation, as depicted in Fig. 1. Therefore, the thinned point process for active APs can be written as:

$$\tilde{\Phi}_{\mathrm{a}} = \left\{ \tilde{x}_i, \tilde{x}_i = \arg\min_{x_i \in \Phi_{\mathrm{a}}} ||x_i - y_j||^2, \forall y_j \in \Phi_{\mathrm{u}} \right\}. \quad (5)$$

Direct current biased orthogonal frequency division multiplexing (DCO-OFDM) is assumed as the modulation format, in which the illumination provided by the LED depends on the DC bias, not on the optical signal. Therefore, idle (inactive) APs are the ones that do not transmit optical signals, but they can be either on (DC bias only) or off, depending on the

illumination requirement. Assume that all active APs transmit with the same signal power, that is P_{tx}. Before VLC signal transmission, the optical signal is clipped at both bottom and upper levels to fit into the linear dynamic range of typical LEDs. To facilitate quantifying the effect of clipping distortion, a parameter ξ is introduced, and it is defined as $\xi = P_{\text{opt}}/\sqrt{P_{\text{tx}}}$, where P_{opt}, set by the DC bias, is the required optical power to meet the illumination requirement. According to the three-sigma rule of thumb, $\xi \geq 3$ ensures that at least 99.7% of the optical signal remains unclipped [21]. To make the analysis tractable and, more importantly, to obtained higher SINR of the communication link, we assume in the paper that the signal power satisfies $P_{\text{tx}} \leq P_{\text{opt}}^2/9$ so that the effect of clipping distortion is negligible. Focusing on the typical user, its received interference power is the sum of received powers from all other active APs other than its serving AP. Also, we assume that there is no intra-cell interference, for example, due to the use of orthogonal multiuser access schemes within each Voronoi cell. Therefore, the SINR at the typical user is given by:

$$\mathsf{SINR} = \frac{P_{\text{tx}}\alpha^2(x_0^2 + L^2)^{-(m+3)}}{\sum\limits_{x_i \in \tilde{\Phi}_{\text{a}} \setminus \{x_0\}} P_{\text{tx}}\alpha^2(x_i^2 + L^2)^{-(m+3)} + \sigma^2}, \tag{6}$$

where σ^2 is the receiver noise power including both shot noise and thermal noise. For such small-scaled VLC networks, user performance is typically limited by the interference cause by neighboring APs rather than the noise process at the receiver end. In this case, the SINR can be well approximated by the SIR:

$$\mathsf{SIR} = \frac{(x_0^2 + L^2)^{-(m+3)}}{\sum\limits_{x_i \in \tilde{\Phi}_{\text{a}} \setminus \{x_0\}} (x_i^2 + L^2)^{-(m+3)}}. \tag{7}$$

The goal of this paper is to evaluate the coverage probability of a typical user in the network, which is equivalent to evaluating the complementary cumulative distribution function (CCDF) of the SINR (or SIR in the interference-limited case). The major difficulty resides in characterizing $\tilde{\Phi}_{\text{a}}$ because the probability density function (PDF) of the Voronoi cell in PPP still remains unknown [15], [22]–[24]. With this in mind, we simplify the problem by making the following assumption.

Assumption 1: The point process for active APs, $\tilde{\Phi}_{\text{a}}$, is a homogeneous PPP, whose intensity is given by $\tilde{\lambda}_{\text{a}} = (1 - p_{\text{idle}})\lambda_{\text{a}}$, where p_{idle} represents the idle probability of APs in the network that are not associated with any users.

In the following, we calculate the idle probability of APs in Section III. In Section IV, we derive analytical results for the coverage probability based on Assumption 1. The accuracy of the obtained results built upon this assumption is later justified in Section V.

III. Idle Probability of APs

Consider a Voronoi cell $\mathcal{A} \subset \mathbb{R}^2$ generated from PPP Φ_{a}. We are interested in finding the probability that there exist k users inside $\mathcal{A}$:

$$\mathbb{P}\left[\sum_{y_i \in \Phi_{\text{u}}} \mathbf{1}_{\mathcal{A}}(y_i) = k\right] = \mathbb{E}_{\mathcal{A}}\left[\frac{(\lambda_{\text{u}}\mu(\mathcal{A}))^k}{k!}\exp\left(-\lambda_{\text{u}}\mu(\mathcal{A})\right)\right], \tag{8}$$

where $\mu(\mathcal{A})$ is the standard Lebesgue measure of $\mathcal{A}$, and $\mathbf{1}_{\mathcal{A}}(y_i)$ is the random counting measure of $\mathcal{A}$, defined as:

$$\mathbf{1}_{\mathcal{A}}(y_i) = \begin{cases} 1, & y_i \in \mathcal{A} \\ 0, & \text{otherwise} \end{cases}. \tag{9}$$

Although the exact PDF of $\mu(\mathcal{A})$ is unknown, existing studies have reported that it can be well approximated with a Gamma distribution $\mu(\mathcal{A}) \sim \text{Gamma}(\beta, \beta\lambda_{\text{a}})$, whose PDF is given by [22]:

$$f_{\mu(\mathcal{A})}(t) = \frac{(\beta\lambda_{\text{a}})^\beta}{\Gamma(\beta)} t^{\beta-1}\exp\left(-\beta\lambda_{\text{a}}t\right), \tag{10}$$

where $\Gamma(\cdot)$ is the gamma function, and the shape parameter $\beta = 3.5$ [22] is obtain through curve fitting. With this approximated PDF, (8) can be calculated as:

$$\begin{aligned}\mathbb{P}\left[\sum_{y_i \in \Phi_{\text{u}}} \mathbf{1}_{\mathcal{A}}(y_i) = k\right] &= \int_0^\infty \frac{(\lambda_{\text{u}}t))^k}{k!}\exp\left(-\lambda_{\text{u}}t\right) f_{\mu(\mathcal{A})}(t)\mathrm{d}t \\ &= \frac{1}{k!}\frac{\Gamma(\beta+k)}{\Gamma(\beta)}\left(\frac{\beta}{\beta+\frac{\lambda_{\text{u}}}{\lambda_{\text{a}}}}\right)^\beta\left(\frac{\frac{\lambda_{\text{u}}}{\lambda_{\text{a}}}}{\beta+\frac{\lambda_{\text{u}}}{\lambda_{\text{a}}}}\right)^k. \end{aligned} \tag{11}$$

The idle probability of APs can be obtained by plugging $k = 0$ into (11), yielding:

$$p_{\text{idle}} = \mathbb{P}\left[\sum_{y_i \in \Phi_{\text{u}}} \mathbf{1}_{\mathcal{A}}(y_i) = 0\right] = \left(\frac{\beta}{\beta + \frac{\lambda_{\text{u}}}{\lambda_{\text{a}}}}\right)^\beta. \tag{12}$$

It can be seen from (12) that the idle probability of APs is determined by the ratio of user density to AP density, but not the exact value of user density or AP density.

Remark 1: By applying Jensen's inequality, the idle probability of APs is lower bounded by $\exp(-\lambda_{\text{u}}/\lambda_{\text{a}})$. This result follows from $p_{\text{idle}} = \mathbb{E}_{\mathcal{A}}[\exp(-\lambda_{\text{u}}\mu(\mathcal{A}))] \geq \exp\left(-\lambda_{\text{u}}\mathbb{E}_{\mathcal{A}}[\mu(\mathcal{A})]\right)$ and $\mathbb{E}_{\mathcal{A}}[\mu(\mathcal{A})] = \lambda_{\text{a}}^{-1}$.

IV. Coverage Probability Analysis

In this section, we focus on the analysis of the coverage probability of a typical user in the network. Since the distribution function of the SINR exhibits different behaviors at low and high values, we separate the analysis into two regimes: 1) in the low SINR regime, where the SINR target is smaller than one. 2) in the high SINR regime, where the SINR target is larger than one.

A. Asymptotic Analysis of the Coverage Probability in the Low SINR Regime

Assumption 2: The multiuser VLC network under consideration is interference-limited so that the SINR can be well approximated by the SIR.

Remark 2: Assumption 2 plays an important role in simplifying the analysis of the coverage probability in Section IV-A. The validation of Assumption 2 is later justified in Section V through simulation results. However, note that Assumption 2 is not explicitly made when we evaluate the coverage probability in the high SINR regime in Section IV-B.

With Assumption 2, we first study the distribution of the interference-to-signal ratio (ISR) at the typical user, given by $\mathsf{ISR} = \mathsf{SIR}^{-1}$. The Laplace transform of the ISR is given in the following theorem.

Theorem 1: The Laplace transform of the ISR of a typical user is given by:

$$\mathcal{L}_{\mathsf{ISR}}(s) = \frac{1}{\frac{1}{m+3}E_{\frac{m+4}{m+3}}(s) + \Gamma\left(\frac{m+2}{m+3}\right)s^{\frac{1}{m+3}}} \exp\Bigg[-\pi\tilde{\lambda}_{\mathrm{a}}L^2 \times \left(-1 + \frac{1}{m+3}E_{\frac{m+4}{m+3}}(s) + \Gamma\left(\frac{m+2}{m+3}\right)s^{\frac{1}{m+3}}\right)\Bigg], \tag{13}$$

where $E_n(z) = \int_1^\infty \exp(-zt)t^{-n}\mathrm{d}t$ is the exponential integral function [25].

Proof: Please refer to Appendix A. ∎

The denominator of the Laplace transform of the ISR is a strictly increasing function with respect to s because its first order derivative is positive:

$$\frac{\partial(1+W(s))}{\partial s} = -\frac{1}{m+3}E_{\frac{1}{m+3}}(s) + \frac{1}{m+3}\Gamma\left(\frac{m+2}{m+3}\right)s^{-\frac{m+2}{m+3}} > 0, \tag{14}$$

in which function $W(s)$ is defined in (32). Furthermore, the denominator of $\mathcal{L}_{\mathsf{ISR}}(s)$ also satisfies $1+W(0) = 1$. Hence, it is shown that the denominator of the Laplace transform of the ISR has only a single root s^* so that $1 + W(s^*) = 0$. The region of convergence (ROC) of the Laplace transform of the ISR is therefore $\Re(s) > \Re(s^*)$, where $\Re(s)$ denotes the real part of s. From (32), it can be seen that the denominator of the Laplace transform is dependent on the Lambertian order of the AP. In other words, the pole of Laplace transform of ISR changes as the Lambertian order of the AP changes. Although a symbolic expression for s^* is not available, its numerical value can be efficiently calculated using standard mathematical software packages. In Fig. 2, the denominator of $\mathcal{L}_{\mathsf{ISR}}(s)$ is plotted against different values of s. It is verified that the denominator of the Laplace transform is a strictly increasing function of s, and it has a single root on the negative real axis. The numerical value of the pole of $\mathcal{L}_{\mathsf{ISR}}(s)$ is found to be -2.173, -1.847 and -1.658 when the semi-angle of the AP is set to 45°, 60° and 75°, respectively.

From the Laplace transform, the coverage probability of a typical user can be obtained by means of the inverse Laplace transform as follows:

$$\mathbb{P}\left[\mathsf{ISR} > T\right] = 1 - \mathcal{L}^{-1}\left\{\frac{\mathcal{L}_{\mathsf{ISR}}(s)}{s}\right\}(\mathsf{ISR})\Big|_{\mathsf{ISR}=T}. \tag{15}$$

Since $\mathcal{L}_{\mathsf{ISR}}(s)/s$ is a nonstandard Laplace function, the exact expression of its inverse, and hence the coverage probability, is hard to obtain. However, its asymptotic property can be utilized to calculate the coverage probability in the low SIR regime. This is stated in the following corollary.

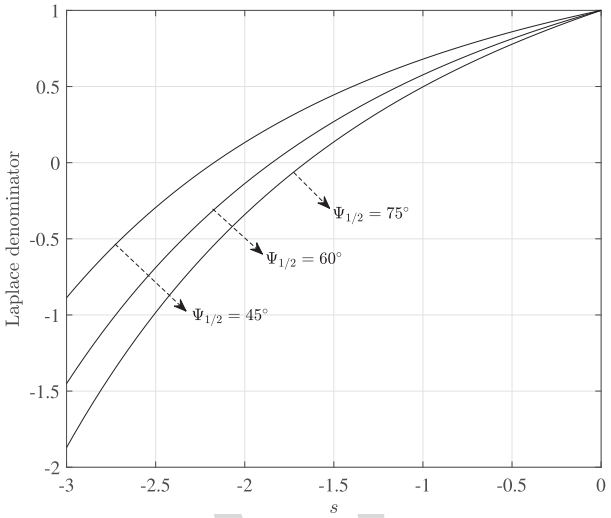

Fig. 2. The denominator of the Laplace transform of the ISR as a function of s.

Corollary 1: The coverage probability of a typical user in the low SIR regime, i.e., $T < 1$, can be approximated by:

$$\mathbb{P}\left[\mathsf{SIR} > T\right] \approx 1 - \exp\left(\frac{s^*}{T}\right), \tag{16}$$

in which s^* is the pole of the Laplace transform of the ISR given in (13).

Proof: The coverage probability can be rewritten as $\mathbb{P}\left[\mathsf{SIR} > T\right] = \mathbb{P}\left[\mathsf{ISR} < 1/T\right]$. Since s^* is a pole of $\mathcal{L}_{\mathsf{ISR}}(s)$, and the abscissa of convergence of the Laplace transform is negative finite, we have the following result from [26]:

$$\lim_{T\to 0^+} T\log\left(\mathbb{P}\left[\mathsf{ISR} > \frac{1}{T}\right]\right) = s^*. \tag{17}$$

For small values of the ISR, (16) can be obtained by rewriting the result in (17). ∎

Remark 3: The pole of the Laplace transform of the ISR does not depend on the parameter L, and therefore the coverage probability of the typical user does not depend on L.

The exponential approximation of the coverage probability in (16) is only valid in the low SIR regime. When $T > 1$, new results for the coverage probability are derived in Section IV-B.

B. Analysis of the Coverage Probability in the High SINR Regime

In this subsection, we focus on evaluating the coverage probability in the high SINR regime. Different from the analysis presented in Section IV-A, here we present more general and exact analysis on the coverage probability by considering both interference and noise in the system model. The derived result complements the result presented in Section IV-A in that it applies to the computation of the coverage probability when $T > 1$, which is a more realistic scenario for practical VLC systems.

From (6), the SINR of a typical user can be simplified to:

$$\mathsf{SINR} = \frac{(x_0^2 + L^2)^{-(m+3)}}{\sum\limits_{x_i \in \tilde{\Phi}_\mathrm{a} \setminus \{x_0\}} (x_i^2 + L^2)^{-(m+3)} + \bar{\sigma}^2}, \tag{18}$$

where the noise power has been normalized to $\bar{\sigma}^2 = \sigma^2 / P_{\mathrm{tx}} \alpha^2$.

Definition 1: Consider two stochastic point processes Φ_1 and Φ_2 for modeling horizontal locations of APs in the VLC network. The SINR models used for Φ_1 and Φ_2 are SINR_1 and SINR_2, respectively. Φ_1 (with SINR_1) is said to be *statistically equivalent* [27] to Φ_2 (with SINR_2) if the distribution of the SINR at the typical user is the same for Φ_1 and Φ_2, i.e., $\mathbb{P}[\mathsf{SINR}_1 > T] = \mathbb{P}[\mathsf{SINR}_2 > T]$. Mathematically, we denote $\Phi_1 \overset{\text{s.e.}}{=} \Phi_2$ and $\mathsf{SINR}_1 \overset{\text{s.e.}}{=} \mathsf{SINR}_2$.

Remark 4: For $\Phi_1 \overset{\text{s.e.}}{=} \Phi_2$, it is sufficient but not necessary that $\Phi_1 = \Phi_2$. However, for $\Phi_1 = \Phi_2$, it is necessary but not sufficient that $\Phi_1 \overset{\text{s.e.}}{=} \Phi_2$.

Since the evaluation of the coverage probability is not straightforward with $\tilde{\Phi}_\mathrm{a}$ and the SINR model given in (18), with Definition 1, we can now focus on analyzing another point process with a more tractable SINR model, as long as both point processes are statistically equivalent.

Theorem 2: The two-dimensional homogeneous PPP $\tilde{\Phi}_\mathrm{a}$, with density $\tilde{\lambda}_\mathrm{a}$ and the SINR model given in (18), is statistically equivalent to another one-dimensional point process $\tilde{\Phi}_\mathrm{eq}$, whose density function is:

$$\tilde{\lambda}_\mathrm{eq}(x) = \frac{\pi \tilde{\lambda}_\mathrm{a}}{\Gamma\left(\frac{1}{m+3}\right)} x^{\frac{1}{m+3}-1}, \tag{19}$$

for $x > L^{2(m+3)}$, and zero otherwise. The equivalent SINR model for $\tilde{\Phi}_\mathrm{eq}$ is:

$$\mathsf{SINR}_\mathrm{eq} = \frac{g_0 x_0^{-1}}{\sum\limits_{x_i \in \tilde{\Phi}_\mathrm{eq} \setminus \{x_0\}} g_i x_i^{-1} + \bar{\sigma}^2}, \tag{20}$$

where g_i, $i = 0, 1, \cdots$, are auxiliary random variables that are exponentially distributed with unity mean, i.e., $g_i \sim \exp(1)$.

Proof: Please refer to Appendix B. ∎

Remark 5: For the original SINR model given in (18), x_i, for $i = 0, 1, \cdots$, takes values between interval $[0, \infty]$. However, for the equivalent SINR model given in (20), x_i, for $i = 0, 1, \cdots$, takes values between interval $\left[L^{2(m+3)}, \infty\right]$. This should be treated carefully when using the density function (19).

Remark 6: Other distributions can also be assumed for auxiliary random variables g_i. However, this requires a recalculation of the density function $\tilde{\lambda}_\mathrm{eq}(x)$ in order to maintain the statistical equivalence.

Although Theorem 2 transforms the original homogeneous two-dimensional PPP $\tilde{\Phi}_\mathrm{a}$ into an inhomogeneous PPP $\tilde{\Phi}_\mathrm{eq}$, it also transforms the original SINR expression in (18) with a Euclidean distance path-loss model into a new SINR expression in (20) with a planar distance path-loss model, multiplied by auxiliary random variables g_i, which mimics the small-scale fading effect in RF based cellular networks. It will be shown in the following analysis that this statistical-equivalent transformation can significantly simplify the calculation of the coverage probability in VLC networks. Specifically, with exponentially distributed auxiliary random variables g_i, the calculation of the coverage probability can now be expressed as a function of exponential terms, which was not possible for the no-fading case in (18).

Based on the statistical-equivalent SINR model given in (20), we have the following result for the coverage probability of a typical user in the network.

Theorem 3: When the SINR target is greater than one, i.e., $T > 1$, the coverage probability of a typical user in the network is given by:

$$\begin{aligned}\mathbb{P}\left[\mathsf{SINR} > T\right] = \int_{L^{2(m+3)}}^{\infty} & \frac{\pi \tilde{\lambda}_\mathrm{a}}{\Gamma\left(\frac{1}{m+3}\right)} x^{\frac{1}{m+3}-1} \exp\left(-T\bar{\sigma}^2 x\right) \\ & \times \exp\left[-\frac{\pi \tilde{\lambda}_\mathrm{a}}{m+2} \frac{L^{-2(m+2)}}{\Gamma\left(\frac{m+4}{m+3}\right)} T x \right. \\ & \left. \times {}_2F_1\left(1, \frac{m+2}{m+3}; \frac{2m+5}{m+3}; -L^{-2(m+3)} T x\right)\right] \mathrm{d}x, \end{aligned} \tag{21}$$

where ${}_2F_1(\cdot, \cdot; \cdot; \cdot)$ denotes the Gauss hypergeometric function [25].

Proof: Please refer to Appendix C. ∎

When the SINR threshold does not satisfy $T > 1$, (21) does not hold because $\mathbb{P}[\mathsf{SINR} > T] < \sum_{i=0}^{\infty} \mathbb{P}[\mathsf{SINR}_i > T]$. In this case, the analytical expression derived in (21) serves as an upper bound on the coverage probability of a typical user. Due to the involved Gauss hypergeometric function, a closed-form expression for the coverage probability is not available. However, the coverage probability can still be computed using numerical methods. In Appendix D, we provide a numerical method for efficient computation of (21).

Remark 7: When $L = 0$, (21) can not be applied. However, in this case, Theorem 3 still holds, and the coverage probability of a typical user can be calculated by $\lim_{L \to 0} \mathbb{P}[\mathsf{SINR} > T]$.

In fact, when $L = 0$, another simpler expression for the coverage probability is available:

$$\begin{aligned}\mathbb{P}\left[\mathsf{SINR} > T\right] = \int_{0}^{\infty} & \frac{\pi \tilde{\lambda}_\mathrm{a}}{\Gamma\left(\frac{1}{m+3}\right)} x^{\frac{1}{m+3}-1} \exp\left(-T\bar{\sigma}^2 x\right) \\ & \times \exp\left[-\pi \tilde{\lambda}_\mathrm{a} \Gamma\left(\frac{m+2}{m+3}\right) (Tx)^{\frac{1}{m+3}}\right] \mathrm{d}x. \end{aligned} \tag{22}$$

Furthermore, significant simplification is possible for the interference-limit case, i.e., when $\bar{\sigma}^2 = 0$. The simplified result for this case is given in the following corollary.

Corollary 2: When $L = 0$, the coverage probability in the interference-limited scenario follows a power-law decay profile:

$$\mathbb{P}\left[\mathsf{SINR} > T\right] = \frac{1}{\Gamma\left(\frac{m+2}{m+3}\right) \Gamma\left(\frac{m+4}{m+3}\right)} T^{-\frac{1}{m+3}}. \tag{23}$$

Proof: This result follows directly from (22) after setting $\bar{\sigma}^2 = 0$. ∎

C. An Upper Bound on the Coverage Probability

Considering the SINR model given in (18), the coverage probability of a typical user can also be calculated in a brute-force way:

$$\mathbb{P}\left[\mathsf{SINR} > T\right] = \int \cdots \int_{D(T)} f_{x_0,x_1,\cdots,x_n}(x_0, x_1, \cdots, x_n)\mathrm{d}x_0\mathrm{d}x_1\cdots\mathrm{d}x_n, \tag{24}$$

where $D(T)$, as a function of the SINR target T, is the domain of integration formed by the $n+1$ variables according to the inequality $\mathsf{SINR} > T$, and $f_{x_0,x_1,\cdots,x_n}(x_0, x_1, \cdots, x_n)$ is the joint distance distribution of the nearest $n+1$ APs in the PPP [28]. Since the domain of integration is highly coupled by $x_0, x_1, \cdots, x_n$, it is typically hard to compute the coverage probability directly with (24). To simplify the problem, we consider only the serving AP x_0 and the nearest interfering AP to the typical user, i.e., x_1. The obtained result therefore serves as an upper bound on the coverage probability since it ignores the effect of receiver noise and underestimates the interference level and hence overestimates the SINR. This result is stated in the following proposition.

Proposition 1: An upper bound on the coverage probability of a typical user is:

$$\mathbb{P}\left[\mathsf{SINR} > T\right] \leq T^{-\frac{1}{m+3}} \exp\left(-\pi\tilde{\lambda}_{\mathrm{a}}L^2\left(T^{\frac{1}{m+3}}-1\right)\right). \tag{25}$$

Proof: Based on the SINR expression given in (18), we have $\mathsf{SINR} \leq (x_0^2+L^2)^{-(m+3)}/(x_1^2+L^2)^{-(m+3)}$ after ignoring the power of interference generated from $\tilde{\Phi}_{\mathrm{a}}\backslash\{x_0, x_1\}$. It immediately follows that $\mathbb{P}[\mathsf{SINR} > T] \leq \mathbb{P}\left[(x_0^2+L^2)^{-(m+3)}/(x_1^2+L^2)^{-(m+3)} > T\right] = \mathbb{P}\left[x_1 > \sqrt{T^{\frac{1}{m+3}}(x_0^2+L^2)-L^2}\right]$. Given that the joint PDF of x_0 and x_1 is $f_{x_0,x_1}(x_0, x_1) = \exp(-\pi\tilde{\lambda}_{\mathrm{a}}x_1^2)(2\pi\tilde{\lambda}_{\mathrm{a}})^2x_0x_1$ [28], we have:

$$\mathbb{P}\left[x_1 > \sqrt{T^{\frac{1}{m+3}}(x_0^2+L^2)-L^2}\right] = \int_0^{\infty}\int_{\sqrt{T^{\frac{1}{m+3}}(x_0^2+L^2)-L^2}}^{\infty} f_{x_0,x_1}(x_0, x_1)\mathrm{d}x_1\mathrm{d}x_0. \tag{26}$$

Calculating the double integral in (26) yields the upper bound expression given in (25). ■

Remark 8: The derivation of this upper bound does not necessarily require $T > 1$. However, it is not meaningful to apply this upper bound to low SINR regimes since for $T \leq 1$ it is definite that $T^{-\frac{1}{m+3}} \exp\left(-\pi\tilde{\lambda}_{\mathrm{a}}L^2\left(T^{\frac{1}{m+3}}-1\right)\right) \geq 1$.

V. Simulation Results and Discussions

Monte Carlo simulation results are presented in this section to validate the theoretical results derived in the previous section. The impacts of previously made assumptions on the accuracy of the results are also discussed. An indoor office of size $18\times14\times3.5$ m^3 is considered, as depicted in Fig. 1. If not otherwise specified, the following parameters are used for the simulation setup. The VLC APs have a semi-angle of 60°, and all active APs transmit at the same power level, that is 1 W.

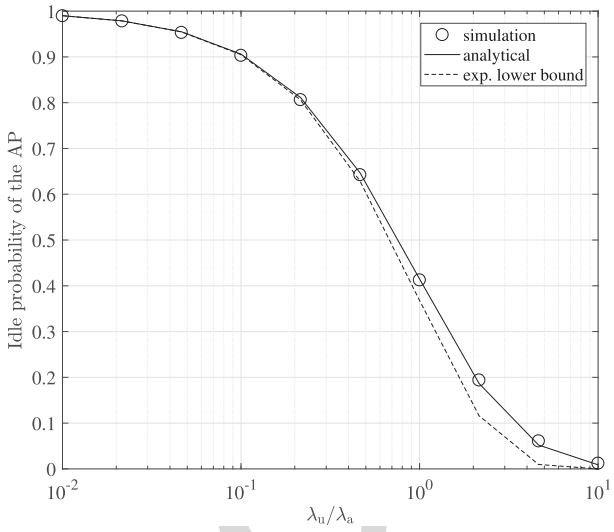

Fig. 3. Idle probability of the AP in the VLC network. $\lambda_{\mathrm{a}} = 0.1$.

The PD used at the receiver side has 90° FOV, an effective detection area of 1 cm^2, and a responsivity of 0.4 A/W. Despite the bandwidth limitation of commercially available white LEDs, current works have shown that using a blue optical filter at the receiver front end can achieve an increased modulation bandwidth of up to 20 MHz [29], [30]. Therefore, a modulation bandwidth of 20 MHz and a noise power spectral density of 10^{-22} A^2/Hz (after blue filtering) [1], [2], [6] is assumed in the simulation. The typical value of the receiver noise power is therefore -117.0 dBm. At the receiver front end, the optical concentrator has a reflective index of 1.5, and the optical filter has a unity gain.

First, based on the highest channel gain association, the idle probability of APs in a typical Voronoi cell is evaluated and the results are shown in Fig. 3. The procedure of calculating the idle probability of the AP using Monte Carlo simulations can be summarized as follows. First, based on the PPP model, generate one realization of independent random locations of APs and users. Second, for each random user, find the AP that gives the highest channel gain based on (4). If, on rare occasions, there are multiple solutions to (4), choose one of the optimal APs randomly. Third, after all users have connected to their optimal APs, count the number of APs that are not connected to any user. The idle probability is therefore calculated as the ratio between the number of unconnected APs and the total number of APs. Finally, generate a large number of realizations, and then calculate the average of the idle probability. It can be seen that analytical results agree well with simulation results, and the exponential lower bound on the idle probability is reasonably accurate, especially when $\lambda_{\mathrm{u}}/\lambda_{\mathrm{a}}$ is small. Fig. 3 also shows that, with given simulation parameters, the idle probability of the AP is nonzero unless $\lambda_{\mathrm{u}} > 10\lambda_{\mathrm{a}}$. Specifically, when the density of users in the network is smaller than the density of APs, i.e., $\lambda_{\mathrm{u}}/\lambda_{\mathrm{a}} \leq 1$, the idle probability is above 0.4. For an underloaded network, e.g., $\lambda_{\mathrm{u}}/\lambda_{\mathrm{a}} = 0.1$, the AP idle probability can be as large as 0.9. Therefore, results in Fig. 3 indicate that considering all of the APs in the network as interfering nodes is inaccurate

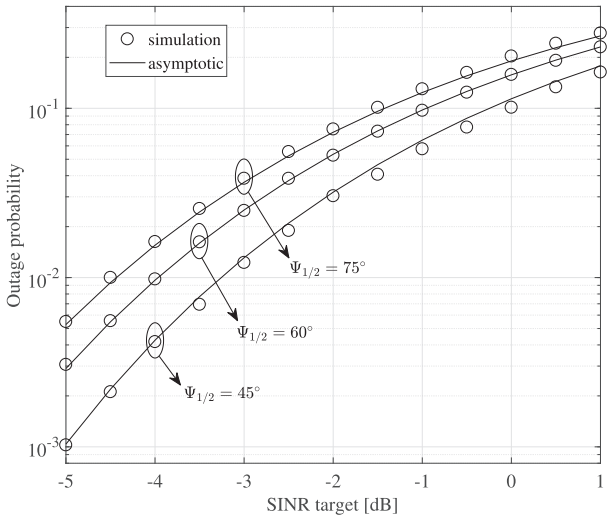

Fig. 4. Outage probability of a typical user in the low SINR regime. $\tilde{\lambda}_{\mathrm{a}} = 0.15$ and $L = 2$ m.

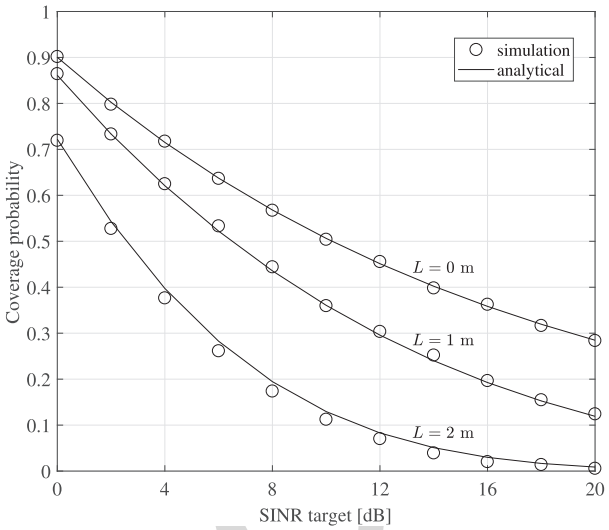

Fig. 5. Coverage probability of a typical user in the high SINR regime. $\tilde{\lambda}_{\mathrm{a}} = 0.1$.

when $\lambda_{\mathrm{u}} < 10\lambda_{\mathrm{a}}$, and this will lead to the underestimation of the coverage performance of users in the network. On the other hand, in an overloaded network where the density of users is about ten times larger than the density of APs, the idle probability of APs can be ignored since its average value approaches zero.

A. Results Based on Assumption 1

In this subsection, we assume that the active APs are a thinned PPP with density $\tilde{\lambda}_{\mathrm{a}} = (1 - p_{\mathrm{idle}})\lambda_{\mathrm{a}}$ (Assumption 1), and discuss the effect of various network parameters on the coverage performance. In Fig. 4, the outage probability[2] of a typical user in the low SINR regime is evaluated. It can be seen that the derived asymptotic expression accurately captures the SINR characteristics when SINR is nearly zero. As the SINR target approaches one, the asymptotic result becomes less accurate. Fig. 4 also shows that using APs with a smaller semi-angle gives better coverage performance at the typical user. This is contradictory to indoor lighting requirements since more uniform illumination would require to install APs with a larger semi-angle. However, this finding is not surprising and can be explained as follows. Although APs with a smaller semi-angle generate more directional light beams, hence less light coverage per AP, they improve the achievable SINR at a typical user because higher signal power and less interference is generated.

Compared to the asymptotic result shown in Fig. 4, the SINR distribution in the high SINR region is typically of more interest. It is shown in Fig. 5 that the derived analytical expression for the coverage probability of a typical user in the high SINR regime is well matched with simulation results. When $L = 0$, the three-dimensional network model reduces to a two-dimensional planar model, and the coverage probability is found to follow a power-law decay profile. When $L \neq 0$,

[2]The outage probability is the complement of the coverage probability. We plot outage probability in Fig. 4 because the coverage probability is less distinguishable when the SINR target is low.

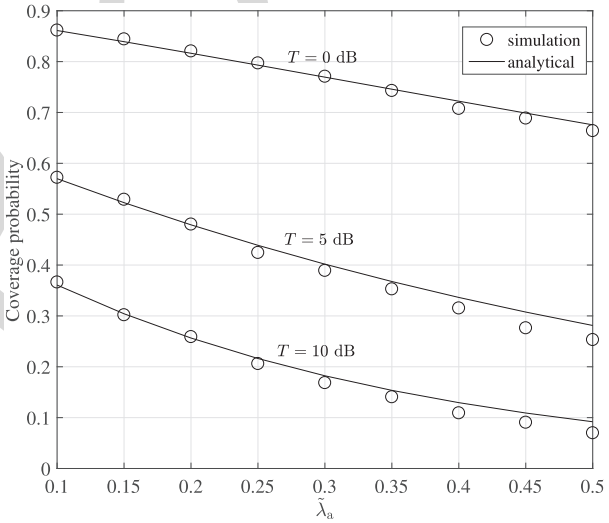

Fig. 6. Coverage probability of a typical user for different densities of the VLC APs. $L = 1$ m.

the coverage probability decay is more involved and it does not follow the power law any more. In fact, the decay is shown to be more rapid at the beginning and steady at the tail.

The impact of the density of APs on the coverage probability of a typical user is evaluated in Fig. 6. As expected, results confirm that, without efficient interference mitigation techniques, the coverage probability reduces as the density of APs increases. This is because that the legitimate user is served by the nearest AP while the increasing number of APs brings an increment of the interference power. However, the decay rate of the coverage probability reduces as the density of active APs increases.

Fig. 7 compares the exact and asymptotic expressions for the coverage probability as a function of parameter L. In general, the coverage probability at a typical user decreases as L increases. The decay of the coverage probability is observed to be steady at small values of L and rapid for large values of L.

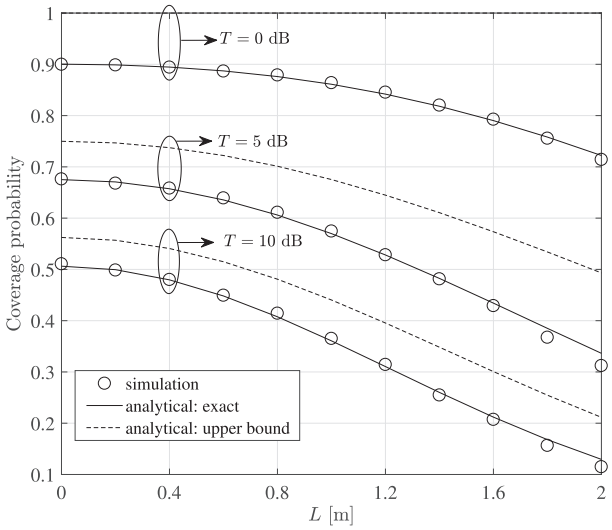

Fig. 7. Coverage probability of a typical user for different values of L. $\tilde{\lambda}_\mathrm{a} = 0.1$.

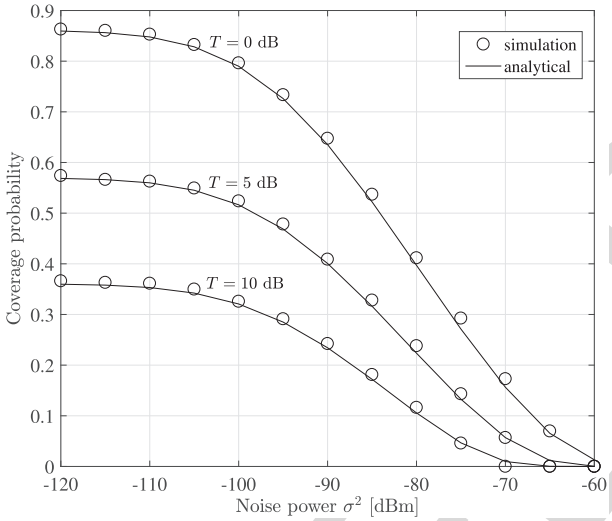

Fig. 8. The impact of noise power on the coverage probability of a typical user. $\tilde{\lambda}_\mathrm{a} = 0.1$ and $L = 1$ m.

The derived analytical expression agrees well with simulation results while the asymptotic expression exhibits a positive gap from the exact one. This gap is caused by underestimating the interference power at the typical user, as stated in Proposition 1. For larger values of T, the gap between the asymptotic result and the exact one becomes tighter. Despite the accuracy of the asymptotic upper bound, it is extremely simple to compute. However, when $T = 0$ dB, this asymptotic upper bound becomes a constant unity bound.

B. Is Assumption 2 Valid?

The asymptotic result shown in Fig. 4 did not consider the effect of receiver noise, but is shown to be reasonably accurate. The analytical results shown in Figs. 5 to 7 did consider the effect of receiver noise, at the cost of being more computationally expensive. So the question is, can the receiver noise be ignored for the coverage analysis in VLC networks (Assumption 2)? To answer this question, in Fig. 8 we evaluate the coverage probability of a typical user with different values of the receiver noise power. It can be seen that, in our simulation setup, the coverage probability is not affected by the receiver noise process, as long as the noise power is below -110 dBm. However, when the power of receiver noise exceeds this threshold, the effect of receiver noise can no longer be ignored, and it starts to deteriorate the coverage performance of a typical user. Fig. 8 also shows that the effect of receiver noise is more dominant when T is small and less dominant when T is large. Nevertheless, the derived analytical result is applicable to the general case with arbitrary noise levels. For typical receiver noise of power -117.0 dBm [1], [6], it is safe to assume that the VLC network is interference-limited, as stated in Assumption 2, and to study the coverage performance using the SIR rather than the SINR.

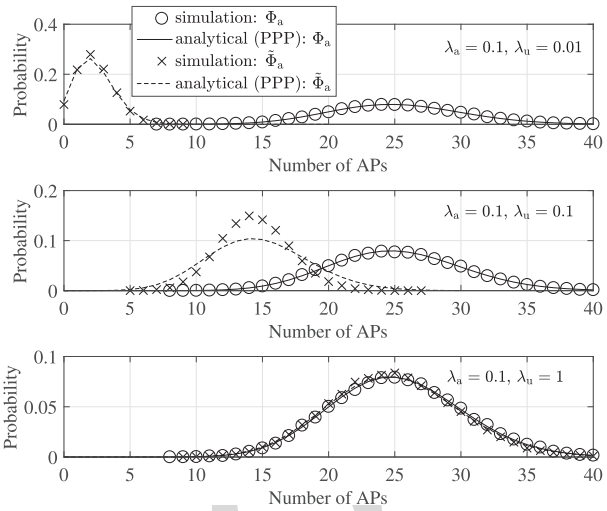

Fig. 9. Probability mass function of Φ_a and $\tilde{\Phi}_\mathrm{a}$.

C. Is Assumption 1 Valid?

In Fig. 3, the derived idle probability of VLC APs is shown to be accurate. However, it does not confirm that the thinned process $\tilde{\Phi}_\mathrm{a}$ is a homogeneous PPP. Therefore, the second question to ask is, is Assumption 1 valid? In order to answer this question, two aspects, namely PPP and homogeneity, need to be studied. In Figs. 9 and 10, we compute the PMF of active APs and compare the exact result with the analytical one (based on Assumption 1). It is shown in Fig. 9 that the number of active APs is not necessarily Poisson-distributed. Specifically, when $\lambda_\mathrm{a} = 0.1$ and $\lambda_\mathrm{u} = 0.01$, the PMF of active APs does follow the Poisson distribution, whose intensity is $\tilde{\lambda}_\mathrm{a} = (1 - p_\mathrm{idle})\lambda_\mathrm{a}$. Mathematically, it is given by:

$$\mathbb{P}\left[\sum_{x_i \in \tilde{\Phi}_\mathrm{a}} \mathbf{1}_{\mathcal{A}}(x_i) = n\right] = \frac{(\tilde{\lambda}_\mathrm{a}\mu(\mathcal{A}))^n}{n!} \exp\left(-\tilde{\lambda}_\mathrm{a}\mu(\mathcal{A})\right), \quad (27)$$

for $n = 0, 1, \cdots$, and zero otherwise. To evaluate the PMF of active APs in the network, $\mathcal{A}$ should be set to the entire (horizontal) area of the indoor environment, so that its standard Lebesgue measure is $\mu(\mathcal{A}) = 18 \times 14$ m^2. The Poisson assumption is also valid when $\lambda_\mathrm{a} = 0.1$ and $\lambda_\mathrm{u} = 1$.

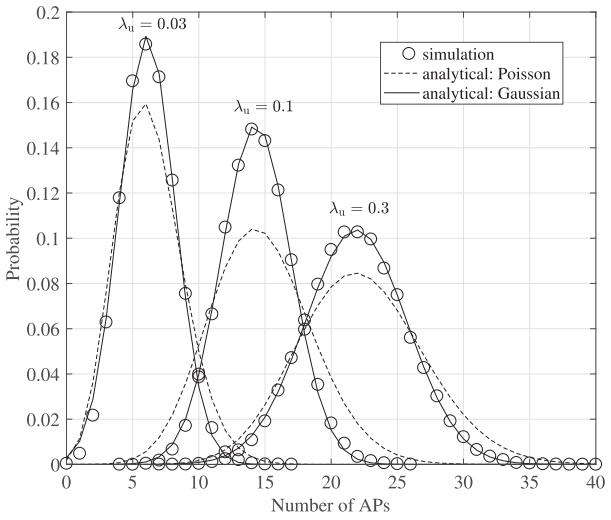

Fig. 10. Gaussian curve fitting for the probability mass function of $\tilde{\Phi}_a$. $\lambda_a = 0.1$.

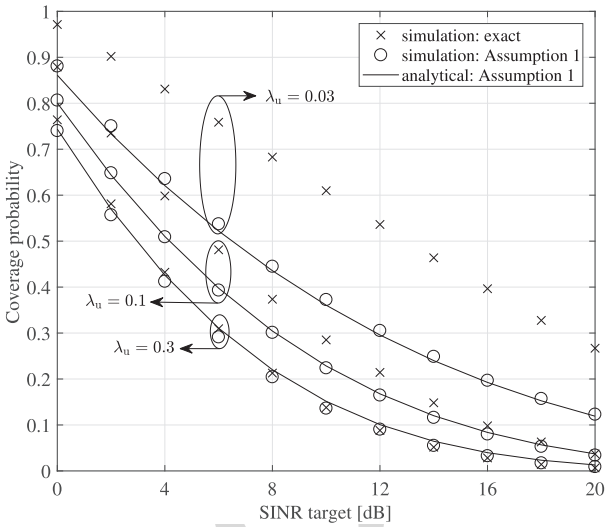

Fig. 11. Coverage probability comparison between the thinned PPP model and the exact results. $\lambda_a = 0.1$ and $L = 2$ m.

TABLE I
GAUSSIAN COEFFICIENTS OBTAINED FROM CURVE FITTING

	a_G	b_G	c_G
$\lambda_u = 0.03$	0.1894	6.093	2.985
$\lambda_u = 0.1$	0.1502	14.32	3.751
$\lambda_u = 0.3$	0.1037	21.89	5.446

In fact, in this case the PMF of active APs is identical to the PMF of all APs in the network since the idle probability is now approximately zero. However, when $\lambda_a = \lambda_u = 0.1$, it is shown that the number of active APs does not follow the PPP anymore, although the actual process and the thinned PPP model have the same mean. Based on these observations, we can conclude from Fig. 9 that the PPP assumption is accurate only when APs and users have distinctive node intensities, or equivalently speaking, when the idle probability of APs is either approximately zero or approximately one. As a rule of thumb, we can say that the PPP assumption is valid when $\lambda_u/\lambda_a \leq 0.1$ or $\lambda_u/\lambda_a \geq 10$, which corresponds to $p_{\text{idle}} \geq 0.91$ or $p_{\text{idle}} \leq 0.01$, respectively (see Fig. 3).

Fig. 9 has showed that the PMF of active APs doe not follow the PPP when λ_a and λ_u are of similar values. To investigate further, we plot in Fig. 10 the PMF of the active APs when $\lambda_a = 0.1$ and $\lambda_u = 0.03, 0.1, 0.3$. This corresponds to $\lambda_u/\lambda_a = 0.3, 1, 3$, respectively. It can be seen from Fig. 10 that number of active APs can be well modeled by the discrete Gaussian distribution, whose PMF is:

$$\mathbb{P}\left[\sum_{x_i \in \tilde{\Phi}_a} \mathbf{1}_{\mathcal{A}}(x_i) = n\right] = a_G \exp\left(-\left(\frac{n - b_G}{c_G}\right)^2\right), \quad (28)$$

where a_G, b_G, c_G are the coefficients obtained from Gaussian curve fitting, that are related to λ_a, λ_u and also the Lebesgue measure of $\mathcal{A}$. For the considered indoor environment, the fitted Gaussian coefficients are summarized in Table I. Although the exact expressions for coefficients a_G and c_G are still unclear, the expression for coefficient b_G can be approximated by $b_G = (1 - p_{\text{idle}})\lambda_a \mu(\mathcal{A})$. This result follows directly from the fact that the Poisson approximation and the Gaussian approximation of the PMF of $\tilde{\Phi}_a$ have the same mean (see Figs. 9 and 10).

To investigate the homogeneity assumption for $\tilde{\Phi}_a$, we show in Fig. 11 the coverage probability of a typical user, comparing the exact result obtained from simulations with the result obtained based on Assumption 1. It is interesting to note that, for a low density of users, the distribution of active APs can be approximated as the PPP, but not a homogeneous one. In fact, a homogeneous PPP assumption will underestimate the coverage probability of a typical user in the network. When the density of users and the density of APs are similar, modeling the active APs in the network as a homogeneous PPP is acceptable since this model only brings small errors to the coverage probability result. When the density of users is larger than the density of APs, for example, in an overloaded network, the homogeneous PPP assumption is found to be very accurate because the idle probability of APs in an overloaded network is approximately zero. Moreover, compared to previous works that do not consider the idleness of APs, e.g., [14], the proposed analytical framework is shown to better capture the characteristics of underloaded networks and certain networks that operate with an AP sleep strategy to save energy and/or minimize the co-channel interference. For overloaded networks, in which the effect of AP idleness can be ignored, the results derived in [14] can also be obtained from the proposed framework by setting λ_u towards infinity.

D. Effect on Room Boundaries

To facilitate analytically tractable derivations, the VLC network is assumed to extend towards infinity, as if there are no boundaries. This assumption does not affect the coverage performance of users located at the cell center. However, this

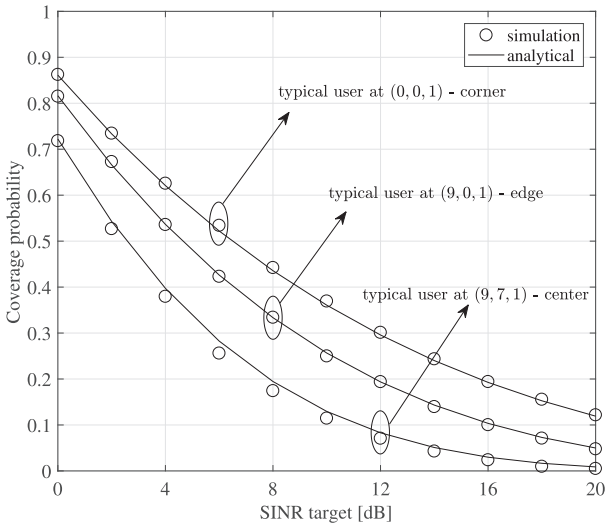

Fig. 12. Coverage probability of a typical user at different locations. $\tilde{\lambda}_{\mathrm{a}} = 0.1$ and $L = 2$ m.

assumption is not valid for users located at the room boundaries, as they generally receive less interference. We show in Fig. 12 that after certain adjustments, the derived analytical expressions are also applicable to users at room boundaries. In particular, the coverage probability of a typical user located at the room edge can still be calculated from Theorem 3 after replacing $\tilde{\lambda}_{\mathrm{a}}$ with $\tilde{\lambda}_{\mathrm{a}}/2$. Similarly, the coverage probability of a typical user located at the room corner can be calculated by replacing $\tilde{\lambda}_{\mathrm{a}}$ with $\tilde{\lambda}_{\mathrm{a}}/4$. It can be seen from Fig. 12 that after adjustment the proposed analytical framework is still accurate.

VI. Conclusions

In this paper, we provide a new analytical framework for the coverage analysis of multiuser VLC networks, taking into account the idle probability of APs that is evident especially in underloaded networks as well as general networks that operate with an AP sleep strategy to save energy and/or minimize the co-channel interference. By using mathematical tools from stochastic geometry and statistical-equivalent transformation, analytical expressions for the coverage probability are derived and given in tractable forms. Based on the derived results, it is shown that not only the density of APs, but also the density of users, has a significant impact on the coverage performance. The homogeneous PPP assumption for active APs is shown to be valid in general and gives close coverage results to the exact ones when the density of users is no smaller than the density of APs. We also show that, for typical receiver noise levels (~ -117.0 dBm), the SINR can be well approximated by the SIR for simplified coverage performance analysis in multiuser VLC networks.

A detailed evaluation of the applicability of the PPP model to VLC networks can be our future work. Further extensions of this work could include more realistic channel and blockage models. It is also of interest to generalize the proposed analytical framework to incorporate cell coordinations.

Appendix

A. Proof of Theorem 1

The Laplace transform of the ISR is formulated as:

$$\begin{aligned}\mathcal{L}_{\mathsf{ISR}}(s) &= \mathbb{E}\left[\exp(-s\mathsf{ISR})\right] \\ &= \mathbb{E}\left[\prod_{x_i\in\tilde{\Phi}_{\mathrm{a}}\setminus\{x_0\}} \exp\left(-s\left(\frac{x_i^2+L^2}{x_0^2+L^2}\right)^{-(m+3)}\right)\right] \\ &= \mathbb{E}_{x_0}\left[\mathbb{E}_{\tilde{\Phi}_{\mathrm{a}}}\left[\prod_{x_i\in\tilde{\Phi}_{\mathrm{a}}\setminus\{x_0\}} \omega(x_i)\,\middle|\, x_0\right]\right], \qquad (29)\end{aligned}$$

in which function $\omega(x_i)$ is defined as $\omega(x_i) = \exp\left(-s\left((x_i^2+L^2)/(x_0^2+L^2)\right)^{-(m+3)}\right)$. With the use of the probability generating functional (PGFL) of the PPP [15], the inner expectation of (29) can be calculated as:

$$\begin{aligned}&\mathbb{E}_{\tilde{\Phi}_{\mathrm{a}}}\left[\prod_{x_i\in\tilde{\Phi}_{\mathrm{a}}\setminus\{x_0\}} \omega(x_i)\,\middle|\, x_0\right] \\ &= \exp\left(-2\pi\tilde{\lambda}_{\mathrm{a}}\int_{x_0}^{\infty} x\,(1-\omega(x))\,\mathrm{d}x\right) \\ &= \exp\left(-\pi\tilde{\lambda}_{\mathrm{a}}\int_1^{\infty}(x_0^2+L^2)\left(1-\exp\left(-sz^{-(m+3)}\right)\right)\mathrm{d}z\right), \qquad (30)\end{aligned}$$

where the last step follows from the change of variable $z = (x^2+L^2)/(x_0^2+L^2)$. Plugging (30) into (29) yields:

$$\begin{aligned}\mathcal{L}_{\mathsf{ISR}}(s) &= 2\pi\tilde{\lambda}_{\mathrm{a}}\int_0^{\infty} x_0 \exp\Bigg[-\pi\tilde{\lambda}_{\mathrm{a}}x_0^2 - \pi\tilde{\lambda}_{\mathrm{a}}\int_1^{\infty}(x_0^2+L^2) \\ &\qquad\times\left(1-\exp\left(-sz^{-(m+3)}\right)\right)\mathrm{d}z\Bigg]\mathrm{d}x_0 \\ &= 2\pi\tilde{\lambda}_{\mathrm{a}}\int_0^{\infty} x_0\exp\left(-\pi\tilde{\lambda}_{\mathrm{a}}x_0^2(1+W(s))\right)\mathrm{d}x_0 \\ &\qquad\times\exp\left(-\pi\tilde{\lambda}_{\mathrm{a}}L^2W(s)\right), \qquad (31)\end{aligned}$$

where function $W(s)$ is defined as:

$$\begin{aligned}W(s) &= \int_1^{\infty}\left(1-\exp\left(-sz^{-(m+3)}\right)\right)\mathrm{d}z \\ &= z\left(1-\frac{1}{m+3}E_{\frac{m+4}{m+3}}\left(sz^{-(m+3)}\right)\right)\Bigg|_{z=1}^{\infty} \\ &= -1+\frac{1}{m+3}E_{\frac{m+4}{m+3}}(s)+\Gamma\left(\frac{m+2}{m+3}\right)s^{\frac{1}{m+3}}. \qquad (32)\end{aligned}$$

Furthermore, the integration (31) can be simplified to:

$$\begin{aligned}&2\pi\tilde{\lambda}_{\mathrm{a}}\int_0^{\infty} x_0\exp\left(-\pi\tilde{\lambda}_{\mathrm{a}}x_0^2(1+W(s))\right)\mathrm{d}x_0 \\ &= -\frac{1}{1+W(s)}\exp\left(-\pi\tilde{\lambda}_{\mathrm{a}}x_0^2(1+W(s))\right)\Bigg|_{x_0=0}^{\infty} \\ &= \frac{1}{1+W(s)}. \qquad (33)\end{aligned}$$

Combining (31) – (33), (13) is obtained.

B. Proof of Theorem 2

Observe from (18) that the SINR model of interest is a function of the distance between the typical user and APs only, but not a function of the azimuth. Therefore, the two-dimensional homogeneous PPP $\tilde{\Phi}_{\mathrm{a}}$, which models the horizontal distance between the typical user and the AP, is statistically equivalent to another one-dimensional inhomogeneous Poisson process $\tilde{\Phi}_{\mathrm{eq1}} = \{x_i, i \in \mathbb{N}\} \subset \mathbb{R}^1$, with density function $\tilde{\lambda}_{\mathrm{eq1}}(x) = \int_0^{2\pi} \tilde{\lambda}_{\mathrm{a}} x \mathrm{d}\theta = 2\pi\tilde{\lambda}_{\mathrm{a}} x$. The SINR model for $\tilde{\Phi}_{\mathrm{eq1}}$ is the same as the one for $\tilde{\Phi}_{\mathrm{a}}$, i.e., $\mathsf{SINR}_{\mathrm{eq1}} = \mathsf{SINR}$. Define a path loss function $\ell(x) = (x^2 + L^2)^{m+3}$, whose inverse can be calculated as $\ell^{-1}(x) = \left(x^{1/(m+3)} - L^2\right)^{1/2}$. Since the path-loss function ℓ has a continuous inverse, this newly mapped process $\tilde{\Phi}_{\mathrm{eq2}} = \{\ell_i, i \in \mathbb{N}\} \subset \mathbb{R}^1$ is also a PPP, generally an inhomogeneous one, according to the mapping theorem [17]. The density function of $\tilde{\Phi}_{\mathrm{eq2}}$, denoted by $\tilde{\lambda}_{\mathrm{eq2}}(\ell)$, can be calculated from the statistical equivalence:

$$\mathbb{E}_{\tilde{\Phi}_{\mathrm{eq2}}}\left[\sum_{\ell_i \in \tilde{\Phi}_{\mathrm{eq2}}} \mathbf{1}_{[\underline{\ell},\bar{\ell}]}(\ell_i)\right] = \mathbb{E}_{\tilde{\Phi}_{\mathrm{eq1}}}\left[\sum_{x_i \in \tilde{\Phi}_{\mathrm{eq1}}} \mathbf{1}_{[\underline{x},\bar{x}]}(x_i)\right], \quad (34)$$

where $[\underline{\ell}, \bar{\ell}]$, with $L^{2(m+3)} \leq \underline{\ell} \leq \bar{\ell}$, is an arbitrary but nonempty interval forming a subset of $\tilde{\Phi}_{\mathrm{eq2}}$, $\underline{x} = \left(\underline{\ell}^{1/(m+3)} - L^2\right)^{1/2}$ and $\bar{x} = \left(\bar{\ell}^{1/(m+3)} - L^2\right)^{1/2}$. Rewriting (34) in terms of the density function for both processes yields:

$$\begin{aligned}\int_{\underline{\ell}}^{\bar{\ell}} \tilde{\lambda}_{\mathrm{eq2}}(\ell)\mathrm{d}\ell &= \int_{\underline{x}}^{\bar{x}} \tilde{\lambda}_{\mathrm{eq1}}(x)\mathrm{d}x \\ &= \int_{\underline{\ell}}^{\bar{\ell}} \tilde{\lambda}_{\mathrm{eq1}}\left(\sqrt{\ell^{\frac{1}{m+3}} - L^2}\right) \frac{1}{m+3} \frac{\ell^{\frac{1}{m+3}-1}}{2\sqrt{\ell^{\frac{1}{m+3}} - L^2}} \mathrm{d}\ell. \quad (35)\end{aligned}$$

From (35), $\tilde{\lambda}_{\mathrm{eq2}}(\ell)$ can be obtained as:

$$\tilde{\lambda}_{\mathrm{eq2}}(\ell) = \frac{\pi\tilde{\lambda}_{\mathrm{a}}}{m+3} \ell^{\frac{1}{m+3}-1}, \quad (36)$$

for $\ell > L^{2(m+3)}$ and zero otherwise. Since the density of $\tilde{\Phi}_{\mathrm{eq2}}$ is found to be a varying function of the distance, it is indeed an inhomogeneous process. Because of the mapping from x to ℓ, the SINR model for $\tilde{\Phi}_{\mathrm{eq2}}$ should be changed accordingly to:

$$\mathsf{SINR}_{\mathrm{eq2}} = \frac{\ell_0^{-1}}{\sum\limits_{\ell_i \in \tilde{\Phi}_{\mathrm{eq2}} \setminus \{\ell_0\}} \ell_i^{-1} + \bar{\sigma}^2}. \quad (37)$$

By letting $\ell^{-1} = g x^{-1}$, we arrive at the SINR model shown in (20). Again, using the mapping theorem [17], we have the following result based on the statistical equivalence property between $\tilde{\Phi}_{\mathrm{eq2}}$ and $\tilde{\Phi}_{\mathrm{eq}}$:

$$\mathbb{E}_{\tilde{\Phi}_{\mathrm{eq2}}}\left[\sum_{\ell_i \in \tilde{\Phi}_{\mathrm{eq2}}} \mathbf{1}_{[\underline{\ell},\bar{\ell}]}(\ell_i)\right] = \mathbb{E}_{g,\tilde{\Phi}_{\mathrm{eq}}}\left[\sum_{x_i \in \tilde{\Phi}_{\mathrm{eq}}} \mathbf{1}_{[\underline{x},\bar{x}]}(x_i)\right], \quad (38)$$

where $\underline{x} = g\underline{\ell}$ and $\bar{x} = g\bar{\ell}$. Furthermore, (38) can be rewritten in the integral form:

$$\begin{aligned}\int_{\underline{\ell}}^{\bar{\ell}} \tilde{\lambda}_{\mathrm{eq2}}(\ell)\mathrm{d}\ell &= \mathbb{E}_g\left[\int_{\underline{x}}^{\bar{x}} \tilde{\lambda}_{\mathrm{eq}}(x)\mathrm{d}x\right] \\ &= \int_{\underline{\ell}}^{\bar{\ell}} \mathbb{E}_g\left[g\tilde{\lambda}_{\mathrm{eq}}(g\ell)\right]\mathrm{d}\ell \\ &= \int_{\underline{\ell}}^{\bar{\ell}} \int_0^{\infty} g\tilde{\lambda}_{\mathrm{eq}}(g\ell)\exp(-g)\mathrm{d}g\mathrm{d}\ell. \quad (39)\end{aligned}$$

After plugging (36) into (39) and using integral equality $\int_0^{\infty} g^{\frac{1}{m+3}}\exp(-g)\mathrm{d}g = \Gamma\left(\frac{m+4}{m+3}\right)$, we have:

$$\begin{aligned}&\int_0^{\infty} g\tilde{\lambda}_{\mathrm{eq}}(g\ell)\exp(-g)\mathrm{d}g \\ &\quad= \int_0^{\infty} \frac{\pi\tilde{\lambda}_{\mathrm{a}}}{m+3} \frac{1}{\Gamma\left(\frac{m+4}{m+3}\right)} \ell^{\frac{1}{m+3}-1} g^{\frac{1}{m+3}}\exp(-g)\mathrm{d}g. \quad (40)\end{aligned}$$

With some simplifications, $\tilde{\lambda}_{\mathrm{eq}}(g\ell)$ can be obtained as:

$$\tilde{\lambda}_{\mathrm{eq}}(g\ell) = \frac{\pi\tilde{\lambda}_{\mathrm{a}}}{m+3} \frac{1}{\Gamma\left(\frac{m+4}{m+3}\right)} (g\ell)^{\frac{1}{m+3}-1}, \quad (41)$$

which is equivalent to (19). To this end, Theorem 2 is proved.

C. Proof of Theorem 3

Based on the statistical equivalence between $\tilde{\Phi}_{\mathrm{a}}$ and $\tilde{\Phi}_{\mathrm{eq}}$, the coverage probability can alternatively be calculated as:

$$\begin{aligned}&\mathbb{P}\left[\mathsf{SINR} > T\right] \\ &= \mathbb{P}\left[\mathsf{SINR}_{\mathrm{eq}} > T\right] \\ &= \mathbb{P}\left[\frac{g_0\, x_0^{-1}}{\sum\limits_{x_i \in \tilde{\Phi}_{\mathrm{eq}} \setminus \{x_0\}} g_i x_i^{-1} + \bar{\sigma}^2} > T\right] \\ &= \mathbb{E}_{g,\tilde{\Phi}_{\mathrm{eq}}}\left[\mathbb{P}\left[g_0 > T x_0 \left(\sum_{x_i \in \tilde{\Phi}_{\mathrm{eq}} \setminus \{x_0\}} g_i x_i^{-1} + \bar{\sigma}^2\right) \middle| x_0\right]\right] \\ &= \mathbb{E}_{g,\tilde{\Phi}_{\mathrm{eq}}}\left[\exp\left(-T\bar{\sigma}^2 x_0\right) \prod_{x_i \in \tilde{\Phi}_{\mathrm{eq}} \setminus \{x_0\}} \exp\left(-T g_i x_i^{-1} x_0\right)\right], \quad (42)\end{aligned}$$

where the last step is obtained from the exponential distribution characteristic of the introduced auxiliary variable g_0. Based on Slivnyak's theorem [15], the calculation of (42) can be simplified by first conditioning on x_0 and then averaging the result with respect to x_0, since conditioning on x_0 does not change the distribution of $x_i \in \tilde{\Phi}_{\mathrm{eq}} \setminus \{x_0\}$. Also, due to the i.i.d. property of g_i and its further independence from $\tilde{\Phi}_{\mathrm{eq}}$, the coverage probability of the typical user can be calculated

with the use of PGFL of the PPP:

$$\mathbb{P}\left[\mathsf{SINR} > T\right] = \mathbb{E}_{x_0}\Bigg[\exp\left(-T\bar{\sigma}^2\, x_0\right)\exp\Bigg[-\int_{L^{2(m+3)}}^{\infty}\tilde{\lambda}_{\mathrm{eq}}(x) \times \left(1-\mathbb{E}_g\left[\exp\left(-Tgx^{-1}x_0\right)\right]\right)\mathrm{d}x\Bigg]\Bigg], \tag{43}$$

in which the inner expectation with respect to the auxiliary variable is found to be:

$$\mathbb{E}_g\left[\exp\left(-Tgx^{-1}x_0\right)\right] = \int_0^{\infty}\exp\left(-Tgx^{-1}x_0\right)\exp(-g)\mathrm{d}g = \frac{1}{1+Tx^{-1}x_0}. \tag{44}$$

Plugging (19) and (44) into (43) yields:

$$\mathbb{P}\left[\mathsf{SINR}>T\right] = \mathbb{E}_{x_0}\left[\exp\left(-T\bar{\sigma}^2x_0\right)\exp\left[-\frac{\pi\tilde{\lambda}_{\mathrm{a}}}{\Gamma\left(\frac{1}{m+3}\right)} \times \int_{L^{2(m+3)}}^{\infty}x^{\frac{1}{m+3}-1}\left(1-\frac{1}{1+Tx^{-1}x_0}\right)\mathrm{d}x\right]\right], \tag{45}$$

in which the inner integration can be calculated as:

$$\int_{L^{2(m+3)}}^{\infty}x^{\frac{1}{m+3}-1}\left(1-\frac{1}{1+Tx^{-1}x_0}\right)\mathrm{d}x = \frac{m+3}{m+2}L^{-2(m+2)}Tx_0{}_2F_1\left(1,\frac{m+2}{m+3};\frac{2m+5}{m+3};-L^{-2(m+3)}Tx_0\right). \tag{46}$$

With a slight abuse of notation, we denote by SINR_i the SINR achieved at the typical user when it receives information signal from AP i and interference from all other APs. It has been shown in (5) that the typical user is associated with the nearest AP in its vicinity. Therefore, we have $\mathsf{SINR} = \mathsf{SINR}_0$. Since $x_0 \le x_1 \le \cdots$ holds by definition, it is straightforward that for $i = 1, 2, \cdots$, $\mathsf{SINR}_i = (x_i^2+L^2)^{-(m+3)} \Big/ \left(\sum_{x_j\in\tilde{\Phi}_{\mathrm{a}}\setminus\{x_i\}}(x_j^2+L^2)^{-(m+3)}+\bar{\sigma}^2\right) < 1$. This is equivalent to $\mathbb{P}[\mathsf{SINR}_i > 1] = 0$. As a result, when $T > 1$, the coverage probability can now be expressed as $\mathbb{P}[\mathsf{SINR} > T] = \mathbb{P}[\mathsf{SINR}_0 > T] = \sum_{i=0}^{\infty}\mathbb{P}[\mathsf{SINR}_i > T]$, which gives:

$$\mathbb{P}\left[\mathsf{SINR} > T\right] = \mathbb{E}_{\tilde{\Phi}_{\mathrm{eq}}}\left[\sum_{x\in\tilde{\Phi}_{\mathrm{eq}}}\exp\left(-T\bar{\sigma}^2x\right)\exp\left[-\frac{\pi\tilde{\lambda}_{\mathrm{a}}}{m+2}\frac{L^{-2(m+2)}}{\Gamma\left(\frac{m+4}{m+3}\right)}Tx \times {}_2F_1\left(1,\frac{m+2}{m+3};\frac{2m+5}{m+3};-L^{-2(m+3)}Tx\right)\right]\right]. \tag{47}$$

After applying Campbell's Theorem [15] and inserting (19) into (47), (21) is obtained.

D. Numerical Computation of the Coverage Probability in (21)

Using the Gauss-Chebyshev Quadrature (GCQ) rule [31], the integration in (21) can be numerically calculated as a finite sum with N_{GCQ} terms:

$$\mathbb{P}\left[\mathsf{SINR}>T\right] \approx \sum_{u=1}^{N_{\mathrm{GCQ}}}w_{(u)}\frac{\pi\tilde{\lambda}_{\mathrm{a}}}{\Gamma\left(\frac{1}{m+3}\right)}x_{(u)}^{\frac{1}{m+3}-1}\exp\left(-T\bar{\sigma}^2x_{(u)}\right) \times \exp\left[-\frac{\pi\tilde{\lambda}_{\mathrm{a}}}{m+2}\frac{L^{-2(m+2)}}{\Gamma\left(\frac{m+4}{m+3}\right)}Tx_{(u)}S_{N_{\mathrm{tol}}}(x_{(u)})\right], \tag{48}$$

where $w_{(u)}$ and $x_{(u)}$, for $u = 1, 2, \cdots, N_{\mathrm{GCQ}}$, are weights and abscissas of the quadrature, respectively [31]. $S_{N_{\mathrm{tol}}}(x_{(u)})$ is the numerical value of the Gauss hypergeometric function evaluated at $x = x_{(u)}$, and it can be computed as follows. From basic Taylor series expansion, the Gauss hypergeometric function at $x_{(u)}$ can be written as [32]:

$$ {}_2F_1\left(1,\frac{m+2}{m+3};\frac{2m+5}{m+3};-L^{-2(m+3)}Tx_{(u)}\right) = \sum_{q=0}^{\infty}\frac{(1)_q\left(\frac{m+2}{m+3}\right)_q}{\left(\frac{2m+5}{m+3}\right)_q}\frac{1}{q!}\left(-L^{-2(m+3)}Tx_{(u)}\right)^q, \tag{49}$$

where $(z)_q$ is the rising Pochhammer symbol, defined as:

$$(z)_q = \begin{cases}1, & q=0,\\ z(z+1)\cdots(z+q-1), & q=1,2,\cdots,.\end{cases} \tag{50}$$

The summation of the first q terms of (49), denoted by $S_q(x_{(u)})$, can be computed through following steps:

$$\begin{aligned}
&S_0(x_{(u)}) = 1,\\
&S_1(x_{(u)}) = \frac{m+2}{2m+5}\left(-L^{-2(m+3)}Tx_{(u)}\right),\\
&\quad q = 2,\\
&\textbf{Do}\quad b_q = \frac{q(m+3)-1}{(q+1)(m+3)-1},\\
&\quad S_q(x_{(u)}) = S_{q-1}(x_{(u)}) + (S_{q-1}(x_{(u)}) - S_{q-2}(x_{(u)})) \times b_q\left(-L^{-2(m+3)}Tx_{(u)}\right),\\
&\quad q = q+1,\\
&\textbf{Until}\ \frac{|S_{N_{\mathrm{tol}}+1}(x_{(u)}) - S_{N_{\mathrm{tol}}}(x_{(u)})|}{|S_{N_{\mathrm{tol}}}(x_{(u)})|} \le \mathrm{tol}\ \&\\
&\quad \frac{|S_{N_{\mathrm{tol}}}(x_{(u)}) - S_{N_{\mathrm{tol}}-1}(x_{(u)})|}{|S_{N_{\mathrm{tol}}-1}(x_{(u)})|} \le \mathrm{tol}\ \&\\
&\quad \frac{|S_{N_{\mathrm{tol}}-1}(x_{(u)}) - S_{N_{\mathrm{tol}}-2}(x_{(u)})|}{|S_{N_{\mathrm{tol}}-2}(x_{(u)})|} \le \mathrm{tol},
\end{aligned}$$

where tol is some tolerance, and $S_{N_{\mathrm{tol}}}(x_{(u)})$ is the returned numerical solution for ${}_2F_1\left(1,\frac{m+2}{m+3};\frac{2m+5}{m+3};-L^{-2(m+3)}Tx_{(u)}\right)$. Note that the maximum number of iterations required for calculating (49) is not fixed. For typical values of T ($0 \le T \le 100$), 200 recursions of q are found to be sufficient for the computation of the coverage probability.

REFERENCES

[1] T. Komine and M. Nakagawa, "Fundamental analysis for visible-light communication system using LED lights," *IEEE Trans. Consum. Electron.*, vol. 50, no. 1, pp. 100–107, Feb. 2004.

[2] J. Grubor, S. Randel, K. D. Langer, and J. W. Walewski, "Broadband information broadcasting using LED-based interior lighting," *J. Lightw. Technol.*, vol. 26, no. 24, pp. 3883–3892, Dec. 15, 2008.

[3] H. Haas, L. Yin, Y. Wang, and C. Chen, "What is LiFi?" *J. Lightw. Technol.*, vol. 34, no. 6, pp. 1533–1544, Mar. 15, 2016.

[4] *IEEE Standard for Local and Metropolitan Area Networks—Part 15.7: Short-Range Wireless Optical Communication Using Visible Light*, IEEE Standard 802.15.7-2011, 2011.

[5] H. Haas, "High-speed wireless networking using visible light," *SPIE Newsroom*, vol. 1, pp. 1–3, Apr. 2013.

[6] L. Zeng *et al.*, "High data rate multiple input multiple output (MIMO) optical wireless communications using white LED lighting," *IEEE J. Sel. Areas Commun.*, vol. 27, no. 9, pp. 1654–1662, Dec. 2009.

[7] B. Li, J. Wang, R. Zhang, H. Shen, C. Zhao, and L. Hanzo, "Multiuser MISO transceiver design for indoor downlink visible light communication under per-LED optical power constraints," *IEEE Photon. J.*, vol. 4, no. 7, Aug. 2015, Art. no. 7201415.

[8] K. Ying, H. Qian, R. J. Baxley, and S. Yao, "Joint optimization of precoder and equalizer in MIMO VLC systems," *IEEE J. Sel. Areas Commun.*, vol. 33, no. 9, pp. 1949–1958, Sep. 2015.

[9] H. Ma, L. Lampe, and S. Hranilovic, "Coordinated broadcasting for multiuser indoor visible light communication systems," *IEEE Trans. Commun.*, vol. 63, no. 9, pp. 3313–3324, Sep. 2015.

[10] M. Kashef, M. Abdallah, K. Qaraqe, H. Haas, and M. Uysal, "Coordinated interference management for visible light communication systems," *J. Opt. Commun. Netw.*, vol. 7, no. 11, pp. 1098–1108, Nov. 2015.

[11] R. Zhang, J. Wang, Z. Wang, Z. Xu, C. Zhao, and L. Hanzo, "Visible light communications in heterogeneous networks: Paving the way for user-centric design," *IEEE Wireless Commun.*, vol. 22, no. 2, pp. 8–16, Apr. 2015.

[12] J. Lian and M. Brandt-Pearce, "Distributed power allocation for multi-user MISO indoor visible light communications," in *Proc. IEEE Global Commun. Conf. (GLOBECOM)*, San Diego, CA, USA, Dec. 2015, pp. 1–7.

[13] D. Bykhovsky and S. Arnon, "Multiple access resource allocation in visible light communication systems," *J. Lightw. Technol.*, vol. 32, no. 8, pp. 1594–1600, Apr. 15, 2014.

[14] C. Chen, D. A. Basnayaka, and H. Haas, "Downlink performance of optical attocell networks," *J. Lightw. Technol.*, vol. 34, no. 1, pp. 137–156, Jan. 1, 2016.

[15] S. N. Chiu, D. Stoyan, W. S. Kendall, and J. Mecke, *Stochastic Geometry and Its Applications*, 2nd ed. Hoboken, NJ, USA: Wiley, 1996.

[16] J. G. Andrews, F. Baccelli, and R. K. Ganti, "A tractable approach to coverage and rate in cellular networks," *IEEE Trans. Commun.*, vol. 59, no. 11, pp. 3122–3134, Nov. 2011.

[17] A. Baddeley, I. Bárány, R. Schneider, and W. Weil, *Stochastic Geometry* (Lecture Notes in Mathematics). Berlin, Germany: Springer-Verlag, 2007.

[18] H. ElSawy, A. Sultan-Salem, M.-S. Alouini, and M. Z. Win, "Modeling and analysis of cellular networks using stochastic geometry: A tutorial," *IEEE Commun. Surveys Tuts.*, vol. 19, no. 1, pp. 167–203, 1st Quart., 2017.

[19] J. M. Kahn and J. R. Barry, "Wireless infrared communications," *Proc. IEEE*, vol. 85, no. 2, pp. 265–298, Feb. 1997.

[20] L. Yin, W. O. Popoola, X. Wu, and H. Haas, "Performance evaluation of non-orthogonal multiple access in visible light communication," *IEEE Trans. Commun.*, vol. 64, no. 12, pp. 5162–5175, Dec. 2016.

[21] S. Dimitrov, S. Sinanovic, and H. Haas, "Clipping noise in OFDM-based optical wireless communication systems," *IEEE Trans. Commun.*, vol. 60, no. 4, pp. 1072–1081, Apr. 2012.

[22] J.-S. Ferenc and Z. Néda, "On the size distribution of Poisson Voronoi cells," *Phys. A, Stat. Mech. Appl.*, vol. 385, no. 2, pp. 518–526, Nov. 2007.

[23] S. Lee and K. Huang, "Coverage and economy of cellular networks with many base stations," *IEEE Commun. Lett.*, vol. 16, no. 7, pp. 1038–1040, Jul. 2012.

[24] C. Li, J. Zhang, and K. B. Letaief, "Throughput and energy efficiency analysis of small cell networks with multi-antenna base stations," *IEEE Trans. Wireless Commun.*, vol. 13, no. 5, pp. 2505–2517, May 2014.

[25] I. S. Gradshteyn and I. M. Ryzhik, *Table of Integrals, Series, and Products*, 7th ed. San Diego, CA, USA: Academic, 2007.

[26] K. Nakagawa, "Application of Tauberian theorem to the exponential decay of the tail probability of a random variable," *IEEE Trans. Inf. Theory*, vol. 53, no. 9, pp. 3239–3249, Sep. 2007.

[27] P. Madhusudhanan, J. G. Restrepo, Y. Liu, T. X. Brown, and K. R. Baker, "Downlink performance analysis for a generalized shotgun cellular system," *IEEE Trans. Wireless Commun.*, vol. 13, no. 12, pp. 6684–6696, Dec. 2014.

[28] H. R. Thompson, "Distribution of distance to Nth neighbour in a population of randomly distributed individuals," *Ecology*, vol. 37, no. 2, pp. 391–394, Apr. 1956.

[29] A. M. Khalid, G. Cossu, R. Corsini, P. Choudhury, and E. Ciaramella, "1-Gb/s transmission over a phosphorescent white LED by using rate-adaptive discrete multitone modulation," *IEEE Photon. J.*, vol. 4, no. 5, pp. 1465–1473, Oct. 2012.

[30] D. Tsonev *et al.*, "Brien, "A 3-Gb/s single-LED OFDM-based wireless VLC link using a gallium nitride μLED," *IEEE Photon. Technol. Lett.*, vol. 26, no. 7, pp. 637–640, Apr. 1, 2014.

[31] M. D. Renzo, "Stochastic geometry modeling and analysis of multi-tier millimeter wave cellular networks," *IEEE Trans. Wireless Commun.*, vol. 14, no. 9, pp. 5038–5057, Sep. 2015.

[32] Y. L. Luke, *The Special Functions and Their Approximations*. New York, NY, USA: Academic, 1969.

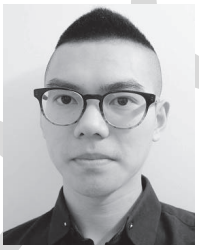

Liang Yin received the B.Eng. degree (Hons.) in electronics and electrical engineering from The University of Edinburgh, Edinburgh, U.K., in 2014, where he is currently pursuing the Ph.D. degree in electrical engineering. His research interests are in visible light communication and positioning, multi-user networking, and wireless network performance analysis. He was a recipient of the Class Medal Award and the IET Prize Award from The University of Edinburgh.

Harald Haas (S'98–AM'00–M'03–SM'17) received the Ph.D. degree from The University of Edinburgh in 2001. He currently holds the Chair of Mobile Communications at The University of Edinburgh, and is the Initiator, Co-Founder, and the Chief Scientific Officer of pureLiFi Ltd., and the Director of the LiFi Research and Development Center, The University of Edinburgh. He has authored 400 conference and journal papers, including a paper in *Science* and co-authored the book *Principles of LED Light Communications Towards Networked Li-Fi* (Cambridge University Press, 2015). His main research interests are in optical wireless communications, hybrid optical wireless and RF communications, spatial modulation, and interference coordination in wireless networks. He first introduced and coined spatial modulation and LiFi. LiFi was listed among the 50 best inventions in *TIME* Magazine 2011. He was an invited speaker at TED Global 2011, and his talk on "Wireless Data from Every Light Bulb" has been watched online over 2.4 million times. He gave a second TED Global lecture in 2015 on the use of solar cells as LiFi data detectors and energy harvesters. This has been viewed online over 1.8 million times. He was elected as a fellow of the Royal Society of Edinburgh in 2017. In 2012 and 2017, he was a recipient of the prestigious Established Career Fellowship from the Engineering and Physical Sciences Research Council (EPSRC) within Information and Communications Technology in the U.K. In 2014, he was selected by EPSRC as one of ten Recognising Inspirational Scientists and Engineers (RISE) Leaders in the U.K. He was a co-recipient of the EURASIP Best Paper Award for the *Journal on Wireless Communications and Networking* in 2015, and co-recipient of the Jack Neubauer Memorial Award of the IEEE Vehicular Technology Society. In 2016, he received the Outstanding Achievement Award from the International Solid State Lighting Alliance. He was a co-recipient of recent best paper awards at VTC-Fall, 2013, VTC-Spring 2015, ICC 2016, and ICC 2017. He is an Editor of the IEEE TRANSACTIONS ON COMMUNICATIONS and the IEEE JOURNAL OF LIGHTWAVE TECHNOLOGIES.